Measurement of prompt D+ and D+s production in pPb collisions at √sNN = 5.02 TeV

Citation: Journal of High Energy Physics. 2024 Jan 15;2024(1):70

As Published: https://doi.org/10.1007/JHEP01(2024)070

Publisher: Springer Berlin Heidelberg

Persistent URL: https://hdl.handle.net/1721.1/153398

Version: Final published version: final published article, as it appeared in a journal, conference proceedings, or other formally published context

Published for SISSA by Springer

Received: *September 27, 2023*
Revised: *December 22, 2023*
Accepted: *January 3, 2024*
Published: *January 15, 2024*

Measurement of prompt D^+ and D_s^+ production in pPb collisions at $\sqrt{s_{\rm NN}} = 5.02$ TeV

The LHCb collaboration

E-mail: yiheng.luo@cern.ch

Abstract: The production of prompt D^+ and D_s^+ mesons is studied in proton-lead collisions at a centre-of-mass energy of $\sqrt{s_{\rm NN}} = 5.02\,\text{TeV}$. The data sample corresponding to an integrated luminosity of $(1.58 \pm 0.02)\text{nb}^{-1}$ is collected by the LHCb experiment at the LHC. The differential production cross-sections are measured using D^+ and D_s^+ candidates with transverse momentum in the range of $0 < p_{\rm T} < 14\,\text{GeV}/c$ and rapidities in the ranges of $1.5 < y^* < 4.0$ and $-5.0 < y^* < -2.5$ in the nucleon-nucleon centre-of-mass system. For both particles, the nuclear modification factor and the forward-backward production ratio are determined. These results are compared with theoretical models that include initial-state nuclear effects. In addition, measurements of the cross-section ratios between D^+, D_s^+ and D^0 mesons are presented, providing a baseline for studying the charm hadronization in lead-lead collisions at LHC energies.

Keywords: Heavy Quark Production, Relativistic Heavy Ion Physics, QCD, Heavy Ion Experiments

ArXiv ePrint: 2309.14206

https://doi.org/10.1007/JHEP01(2024)070

JHEP01(2024)070

Contents

1 Introduction

Quark gluon plasma (QGP) is a new form of matter consisting of deconfined quarks and gluons as basic components at high energy densities [1]. The production of QGP and investigation of its properties are among the primary goals of high energy heavy-ion collision experiments. Heavy quarks are sensitive and effective probes for QGP transport properties, as they are produced in pairs in the early stage of heavy-ion collisions by hard scatterings and experience the entire evolution of the fireball prior to the hadronization process. The measured D-meson nuclear modification factors (R_{AA}) in nucleus-nucleus (AA) collisions at the RHIC [2, 3] and the LHC [4–6] colliders show a strong suppression at high transverse momentum (p_{T}) and demonstrate a significant charm-quark energy loss in the medium [7–10]. This modification factor is calculated as the ratio of D-meson cross-sections from AA to proton-proton (pp) collisions, and is scaled by the binary collision number. The production ratio of strange D_s^+ to non-strange D^0 mesons is found to be enhanced in $\sqrt{s_{\mathrm{NN}}} = 200\,\mathrm{GeV}$ gold-gold collisions [11] and in $\sqrt{s_{\mathrm{NN}}} = 5.02\,\mathrm{TeV}$ lead-lead collisions [12, 13], compared with the results from pp collisions data [14, 15] and PYTHIA pp simulation [16, 17]. This is attributed to the enhanced production of strange quarks in the hot dense medium and charm quark hadronization *via* the coalescence mechanism [18–21]. To fully understand the experimental measurements for nucleus-nucleus collisions, it is essential to characterize the cold nuclear matter (CNM) effects due to the involvement of heavy nuclei like lead in the colliding system.

Multiple CNM effects could modify the heavy-flavor hadron production and kinematic distributions. One way to investigate these effects is to study proton-nucleus (pA) collisions, where it is assumed that QGP effects are not dominant. In the initial state, the nuclear environment influences the parton distribution functions (PDFs) of the bound nucleons, and this modification depends on the parton momentum fraction (Bjorken-x), the momentum transfer squared (Q^2), and the nucleus mass number (A) [22, 23]. At LHC energies and at forward rapidity (corresponding to Bjorken-$x \approx 10^{-6} - 10^{-5}$), the most relevant effect on PDFs is nuclear shadowing [24]. If the gluon phase space is saturated then the D-meson yield, which may be significantly affected at low p_{T}, can be described by the Colour Glass Condensate (CGC) effective theory [25–28].

Measurements of lepton production from semileptonic decays of heavy flavour hadrons in deuteron-gold collisions at the RHIC [29, 30] and in proton-lead (pPb) collisions at the LHC [31–33] suggest that CNM effects are present. These can be further studied with measurements of decays of charm hadrons in pPb collisions at the LHC [34–47]. Recently, the LHCb experiment measured J/ψ [34], $\psi(2S)$ [35], D^0 [36] meson and Λ_c^+ [37] baryon production at $\sqrt{s_{\mathrm{NN}}} = 5.02\,\mathrm{TeV}$ and D-meson production at $\sqrt{s_{\mathrm{NN}}} = 8.16\,\mathrm{TeV}$ [48, 49] in pPb collisions at forward and backward rapidities. The ALICE collaboration also studied the D-meson production in pPb collisions [38, 40, 42, 44] at the same centre-of-mass energy in the rapidity interval $-0.96 < y^* < 0.04$, where y^* is the rapidity of the D mesons in the nucleon-nucleon centre-of-mass frame. Extensive measurements of charm-quark production at low p_{T} have greatly constrained in the PDFs [50, 51], in particular the D^0 results in LHCb pPb collisions [51].

This paper reports measurements of production cross-sections, nuclear modification factors and forward-backward production ratios for prompt D^+ and D_s^+ mesons produced directly in proton-lead interactions or from excited charmed hadron decays. The measurement is performed at $\sqrt{s_{\mathrm{NN}}} = 5.02\,\mathrm{TeV}$ with the LHCb detector [52], which is able to cover two different acceptance regions in the nucleon-nucleon rest frame. In the “forward” (“backward”) configuration, the region is $1.5 < y^* < 4.0$ ($-5.0 < y^* < -2.5$), and the positive direction is defined with respect to the direction of the proton beam. The measurement of the production cross-section is performed over the range of D^+ and D_s^+ transverse momentum $0 < p_{\mathrm{T}} < 14\,\mathrm{GeV}/c$, in both backward and forward configurations. Finally, the production ratios between D^+, D_s^+ and D^0 mesons in pPb collisions are presented as a function of p_{T} and y^*, and compared with the measurements in pp [15, 53] and pPb collisions [38] at same nucleon-nucleon centre-of-mass energy at the LHC.

2 Detector and data samples

The LHCb detector [52, 54] is a single-arm forward spectrometer covering the pseudorapidity range $2 < \eta < 5$, designed for the study of particles containing charm or beauty quarks. The detector includes a high-precision tracking system consisting of a silicon-strip vertex detector surrounding the pp interaction region (VELO), a large-area silicon-strip detector (TT) located upstream of a dipole magnet with a bending power of about 4 Tm, and three stations of silicon-strip detectors (IT) and straw drift tubes (OT) placed downstream of the magnet. The tracking system provides a measurement of momentum, p, of charged particles with a relative uncertainty that varies from 0.5% at low momentum to 1.0% at 200 GeV/c. The minimum distance of a track to a primary interaction vertex (PV), the impact parameter (IP), is measured with a resolution of $(15 + 29/p_{\mathrm{T}})$ µm. Different types of charged hadrons are distinguished using information from two ring-imaging Cherenkov detectors. Photons, electrons and hadrons are identified by a calorimeter system consisting of scintillating-pad and preshower detectors, an electromagnetic calorimeter and a hadronic calorimeter. Muons are identified by a system composed of alternating layers of iron and multiwire proportional chambers [55]. The online event selection is performed by a trigger [56], which consists of a hardware stage, based on information from the calorimeter and muon systems, followed by a software stage, which applies a full event reconstruction.

This analysis uses the pPb data sample collected by the LHCb detector in early 2013, corresponding to integrated luminosities of $(1.06 \pm 0.02)\,\mathrm{nb}^{-1}$ and $(0.52 \pm 0.01)\,\mathrm{nb}^{-1}$ for the forward and backward collisions, respectively [34]. The instantaneous luminosity during the data taking period was about 5×10^{27} cm^{-2} s^{-1}, resulting in event rates three orders of magnitude lower than for typical LHCb pp interactions. Consequently, the hardware trigger only rejected empty events, while the software trigger accepted all events with at least one track reconstructed in the VELO.

Simulated samples of pPb collisions at $\sqrt{s_{\mathrm{NN}}} = 5.02$ TeV are used to determine detector efficiencies. In the simulation, D mesons in pp collisions are generated using Pythia [16, 57], embedded into minimum bias pPb events from the EPOS generator [58] and calibrated with LHC data [59]. Hadronic decays are generated using EvtGen [60], in which final-state radiation is simulated by Photos [61]. The interaction of the generated particles with the LHCb detector, and its response, are implemented using the Geant4 toolkit [62–64].

3 Cross-section determination

The prompt D-meson double-differential production cross-section in a given (p_{T}, y^*) kinematic bin is defined as

$$\frac{\mathrm{d}^2\sigma}{\mathrm{d}p_{\mathrm{T}}\mathrm{d}y^*} = \frac{N(p_{\mathrm{T}}, y^*)}{\mathcal{L}\varepsilon_{\mathrm{tot}}\mathcal{B}\Delta p_{\mathrm{T}}\Delta y^*}. \tag{3.1}$$

In the formula, $N(p_{\mathrm{T}}, y^*)$ is the signal yield of prompt D-meson candidates, $\varepsilon_{\mathrm{tot}}$ is the total detection efficiency in a specific bin of (p_{T}, y^*), $\mathcal{L}$ is the integrated luminosity, $\mathcal{B}$ is the branching fraction of the corresponding D-meson decay and Δp_{T} and Δy^* are the bin widths of the p_{T} and rapidity, respectively. The D-meson candidates are reconstructed through the $D^+ \to K^-\pi^+\pi^+$ or $D_s^+ \to K^-K^+\pi^+$ decay channels,[1] where the mass of the K^+K^- pair in the D_s^+ meson candidate is required to fall within ±20 MeV/c^2 of the known mass of the $\phi(1020)$ meson. The corresponding branching fractions are $\mathcal{B} = (9.38 \pm 0.15)\%$

---

[1] In this paper charge-conjugated processes are implied unless stated otherwise.

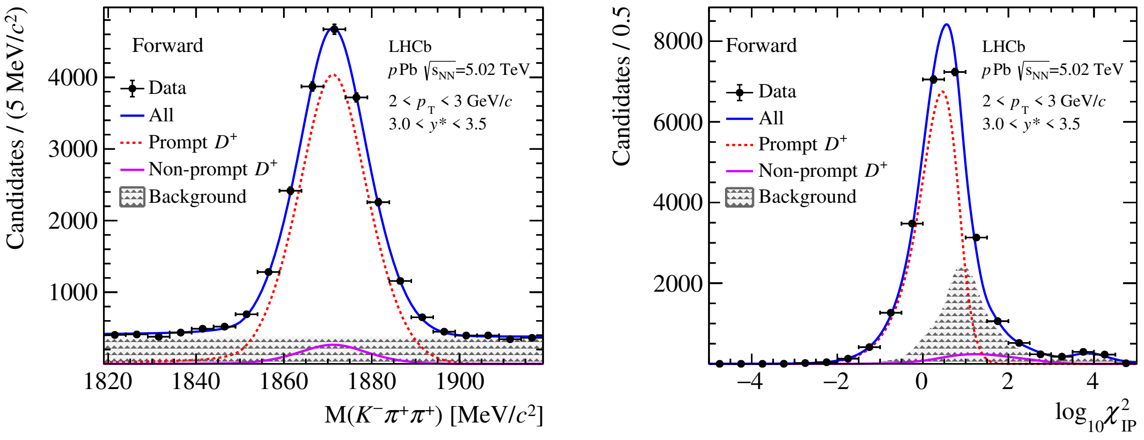

Figure 1. Distributions of the simultaneous fits to the (left) $\mathrm{M}(K^-\pi^+\pi^+)$ and (right) $\log_{10}\chi^2_{\mathrm{IP}}$ for D^+ mesons in the forward data sample in the kinematic bin of $2 < p_{\mathrm{T}} < 3\,\mathrm{GeV}/c$ and $3.0 < y^* < 3.5$.

for the $D^+ \to K^-\pi^+\pi^+$ decay obtained from ref. [65], and $\mathcal{B} = (2.24 \pm 0.13)\%$ for the $D_s^+ \to K^-K^+\pi^+$ decay, obtained from ref. [66].

The total cross-section over a specific kinematic range is determined by integrating the double-differential cross-section. The nuclear modification factor, $R_{p\mathrm{Pb}}$, i.e. the normalized ratio of the D-meson production cross-section in pPb collisions to that in pp interactions at the same nucleon-nucleon centre-of-mass energy is defined as

$$R_{p\mathrm{Pb}}(p_{\mathrm{T}}, y^*) \equiv \frac{1}{A}\frac{\mathrm{d}^2\sigma_{p\mathrm{Pb}}(p_{\mathrm{T}}, y^*)/\mathrm{d}p_{\mathrm{T}}\mathrm{d}y^*}{\mathrm{d}^2\sigma_{pp}(p_{\mathrm{T}}, y^*)/\mathrm{d}p_{\mathrm{T}}\mathrm{d}y^*}, \tag{3.2}$$

where A=208 is the mass number of the lead nucleus. The forward-backward production ratio is defined as

$$R_{\mathrm{FB}}(p_{\mathrm{T}}, y^*) \equiv \frac{\mathrm{d}^2\sigma_{\mathrm{forward}}(p_{\mathrm{T}}, |y^*|; y^* > 0)/\mathrm{d}p_{\mathrm{T}}\mathrm{d}y^*}{\mathrm{d}^2\sigma_{\mathrm{backward}}(p_{\mathrm{T}}, |y^*|; y^* < 0)/\mathrm{d}p_{\mathrm{T}}\mathrm{d}y^*}, \tag{3.3}$$

in the common rapidity region $2.5 < |y^*| < 4.0$.

The D-meson candidates are selected using similar selection criteria to those for the open charm production measurements in pp collisions at $\sqrt{s} = 5.02\,\mathrm{TeV}$ [53], 7 TeV [67] and 13 TeV [68] at LHCb. The trajectories of kaons and pions from the D-meson candidates are required to be of good quality and originate from a common vertex. In order to improve the signal purity, more stringent particle identification (PID) requirements than in pp interactions are exploited.

The prompt and non-prompt (i.e. from b-hadron decays) D-meson yields in intervals of the p_{T} and y^* are determined from simultaneous extended maximum-likelihood fits to the unbinned invariant-mass and $\log_{10}\chi^2_{\mathrm{IP}}$ distributions. Here, χ^2_{IP} is the difference in vertex-fit χ^2 of a given PV reconstructed with and without consideration of the signal candidates. The simultaneous fits are performed to the D-meson candidates whose invariant mass lies within $\pm 50\,\mathrm{MeV}/c^2$ of their known mass [65]. The inclusive signal shape in the $M(K^-\pi^+\pi^+)$ or $M(K^-K^+\pi^+)$ distributions is modeled by the sum of a Crystal Ball (CB) function [69] and a Gaussian with the same mean. The widths of CB function and Gaussian vary freely in the

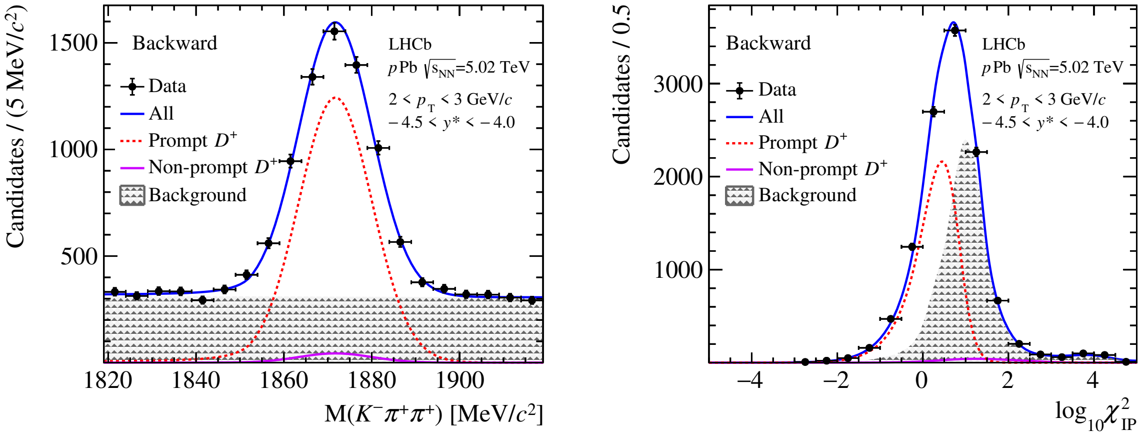

Figure 2. Distributions of the simultaneous fits to the (left) $\mathrm{M}(K^-\pi^+\pi^+)$ and (right) $\log_{10}\chi^2_{\mathrm{IP}}$ for D^+ mesons in the backward data sample in the kinematic bin of $2 < p_{\mathrm{T}} < 3\,\mathrm{GeV}/c$ and $-4.5 < y^* < -4.0$.

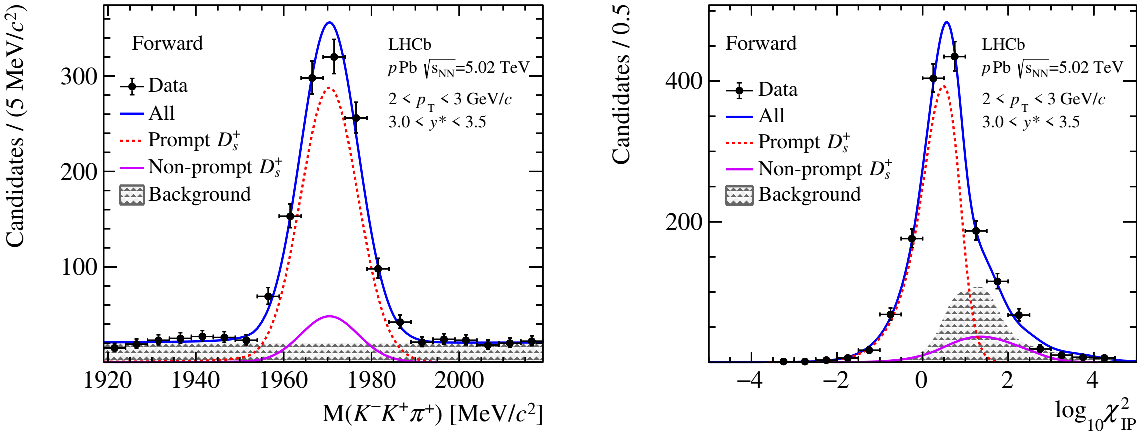

Figure 3. Distributions of the simultaneous fits to the (left) $\mathrm{M}(K^-K^+\pi^+)$ and (right) $\log_{10}\chi^2_{\mathrm{IP}}$ for D_s^+ mesons in the forward data sample in the kinematic bin of $2 < p_{\mathrm{T}} < 3\,\mathrm{GeV}/c$ and $3.0 < y^* < 3.5$.

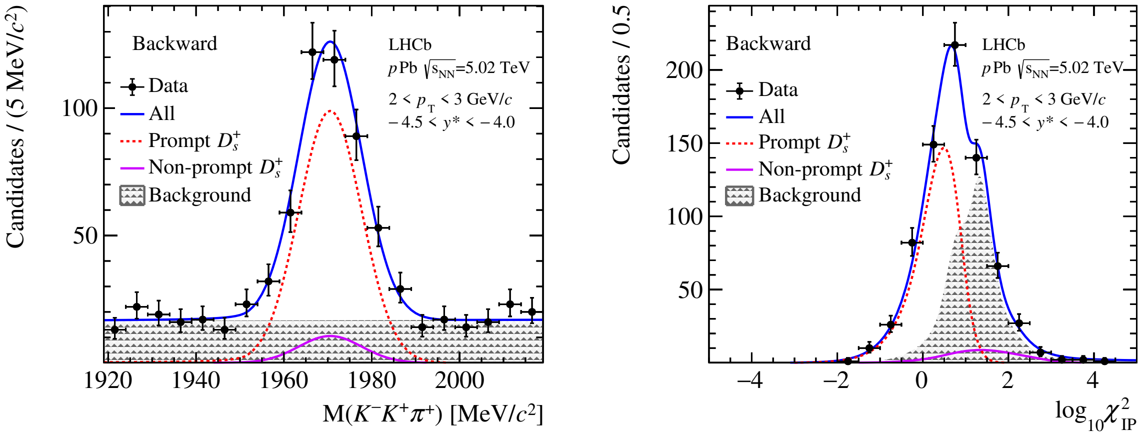

Figure 4. Distributions of the simultaneous fits to the (left) $\mathrm{M}(K^-K^+\pi^+)$ and (right) $\log_{10}\chi^2_{\mathrm{IP}}$ for D_s^+ mesons in the backward data sample in the kinematic bin of $2 < p_{\mathrm{T}} < 3\,\mathrm{GeV}/c$ and $-4.5 < y^* < -4.0$.

fit, and the fraction and the tail parameters of the CB function are fixed to values obtained from simulation. The combinatorial background is described by a linear function. The $\log_{10}\chi^2_{\mathrm{IP}}$ shapes for the prompt and non-prompt D-meson signal candidates are estimated using simulated events and modeled with an asymmetric Bukin curve [70] with tails described by Gaussian functions. In the forward and backward cases for both prompt and non-prompt components, the width, asymmetry and tail coefficients of the Bukin function are fixed to the values obtained from simulated events. Additionally, the Bukin peak location for non-prompt D mesons is fixed to the value obtained from simulated events. The Bukin parameters are determined from the fit to the whole forward or backward simulation sample. The combinatorial background $\log_{10}\chi^2_{\mathrm{IP}}$ distribution is modeled by a kernel density estimate function [71], which is created in the side-band interval outside their $\pm 50\,\mathrm{MeV}/c^2$ mass window. The total model is the sum of the contributions from the prompt and non-prompt signals and the combinatorial background, where each component is the product of the corresponding mass and $\log_{10}\chi^2_{\mathrm{IP}}$ distributions. The simultaneous fits are carried out independently in each (p_{T}, y^*) bin of the D^+ or D_s^+ mesons. Figures 1–4 show the invariant mass and $\log_{10}\chi^2_{\mathrm{IP}}$ distributions, for two typical bins of y^* in the forward and backward regions.

The total efficiency, $\varepsilon_{\mathrm{tot}}$, in eq. (3.1) is the product of the geometric acceptance, trigger, reconstruction, selection, and PID efficiencies. The geometric acceptance efficiency is estimated using simulated *pp* events to eliminate the effect of the spatial acceptance of the LHCb detector. The analysis uses a minimum activity trigger whose efficiency for events containing a D^+ or D_s^+ meson is found to be 100%. The reconstruction and selection efficiencies are calculated with simulated *p*Pb samples at 5.02 TeV, and corrected for known differences in tracking efficiency between data and simulation [72]. The PID efficiency is estimated using a sample of D^0 meson decays selected from data without PID criteria [54], and collected during the same period as the *p*Pb sample used in the analysis. The PID selection efficiency is calculated using the kaon and pion single-track efficiencies from calibration data, and averaging them based on the kinematic distributions observed in the simulated events in each (p_{T}, y^*) bin. The reconstruction and selection efficiency and the PID efficiency are sensitive to differences between the track multiplicity distributions in *p*Pb data and those observed in the simulation and PID-calibration samples. This effect is corrected for by re-weighting the latter to match the distributions seen in data.

4 Systematic uncertainties

The systematic uncertainties affecting the cross-section measurements are listed in table 1. The uncertainties of the forward and backward samples were evaluated separately, unless stated otherwise.

The systematic uncertainty related to the determination of the prompt signal yield has contributions both from the assumed fit model and the fixed parameters in the simultaneous fits, and from the fit method itself. The uncertainty associated to the fit model is assigned using double CB functions for the signal component and an exponential function for the background component to fit the invariant-mass distributions, and using a Gaussian for non-prompt components to fit the $\log_{10}\chi^2_{\mathrm{IP}}$ distributions. Parameters in the fit model are allowed to vary from their nominal values within uncertainties estimated from simulated events. The standard deviation of the nominal and the alternative fits is taken as the

Source	$D^+ \to K^-\pi^+\pi^+$		$D_s^+ \to K^-K^+\pi^+$	
	Forward	Backward	Forward	Backward
Uncorrelated between bins				
Prompt yield determination	0.1–1.4	0.1–0.9	0–3.4	0–6.5
Simulation sample size	0–10	0–8	1–8	1–6
Correlated between bins				
Multiplicity correction	0.4–2.3	1.8–4.8	0.4–2.5	2.1–5.0
Hadronic interactions	3.9	3.9	3.6	3.6
PID efficiency	0–18	1–13	1–12	1–17
Luminosity	1.9	2.1	1.9	2.1
Branching fraction	1.6	1.6	5.8	5.8
Statistical uncertainty	1–20	1–28	3–48	4–52

Table 1. Summary of systematic and statistical uncertainties on the D-meson cross-section measurements (%).

uncertainty on the prompt signal yield determination. The resulting uncertainty is estimated to be less than 6.5% for most bins.

The systematic uncertainty related to the multiplicity correction of the reconstruction and selection efficiencies is due to several contributions. One source of uncertainty is caused by the choice of the variables used to represent the detector occupancy for weighting the distribution. The number of charged tracks, the number of long tracks, the number of hits in the VELO, the number of hits in the IT and the OT, and the number of hits in the TT, are all considered separately. The standard deviation of the efficiencies weighted by each variable is taken as systematic uncertainty. The effects are summed in quadrature, yielding a total uncertainty on the D^+ (D_s^+) meson multiplicity correction of $0.4 - 2.3\%$ ($0.4 - 2.5\%$) and $1.8 - 4.8\%$ ($2.1 - 5.0\%$) for the forward and backward collision samples, respectively.

The difference in tracking efficiencies between data and simulation is studied with muons. An additional uncertainty of 1.1% (1.4%) is assigned for each kaon (pion) present in the final state, due to the incomplete modeling of the hadronic interactions of these particles with the material of the LHCb detector [36]. This effect is dominated by the uncertainty on knowledge of the amount of material present within the detector and hence can be assumed to be fully correlated for kaons and pions. The total uncertainty associated to this effect is 3.9% (3.6%) for D^+ (D_s^+) mesons.

The finite size of the calibration sample used to determine the particle identification efficiency also contributes to the systematic uncertainty. This contribution is evaluated by varying the pion and kaon PID efficiencies obtained from the calibration sample within

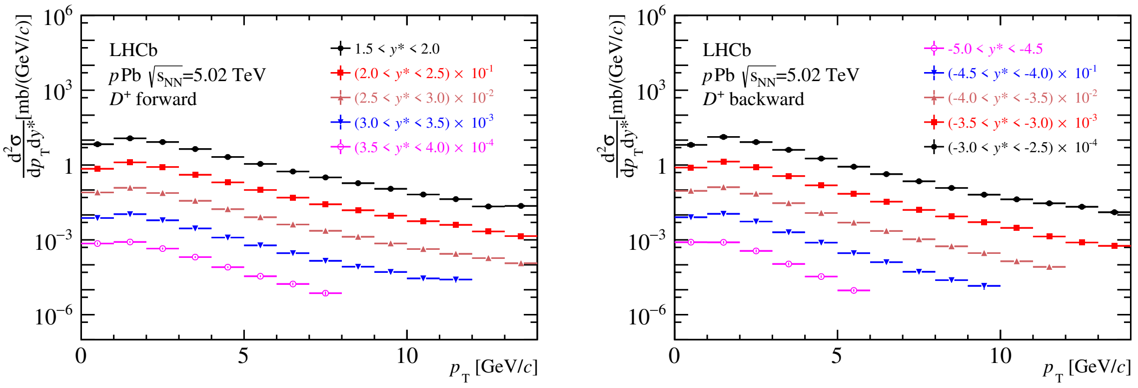

Figure 5. Double-differential cross-section of prompt D^+ mesons in pPb collisions for the (left) forward and (right) backward rapidities. The error bars are the statistical uncertainty and the boxes are the systematic uncertainty, both of which are smaller than the symbol size. The value in a particular rapidity interval is scaled by a multiplicative factor 10^{-m}, where the factor m increase as the rapidity rises.

their statistical uncertainties. The uncertainty from the PID binning scheme is studied by using alternative binning schemes for the single track efficiency. The total PID systematic uncertainty is a quadratic sum of these two sources and it ranges between 0 and 18% depending on the kinematic region and the collision sample.

The relative uncertainty of the integrated luminosity is nearly 2% for both forward and backward samples [34]. The relative uncertainty of the branching fraction is 1.6% [65] and 5.8% [66] for $\mathcal{B}(D^+ \to K^-\pi^+\pi^+)$ and $\mathcal{B}(D_s^+ \to K^-K^+\pi^+)$, respectively. The finite size of the simulation sample introduces uncertainties on the efficiencies which are then propagated to the cross-section measurements. This effect is negligible for the central rapidity region, while becomes significant in the region close to the boundaries of p_{T} and y^*, ranging between 0 and 10%. The total systematic uncertainty varies gradually from 5% in the central rapidity interval to about 20% in the boundary interval.

5 Results

5.1 Production cross-sections

The measured values of the double-differential cross-section of prompt D^+ and D_s^+ mesons in proton-lead collisions for forward and backward rapidities, as a function of p_{T} and y^*, are displayed in figures 5 and 6 and summarized in tables 2–5 of appendix A.

The one-dimensional differential prompt D^+ and D_s^+ meson cross-sections as a function of p_{T} or y^* are shown in figures 7 and 8, and are also summarized in appendix A. The measurements are also shown as a function of p_{T} integrated over y^* for the common rapidity range $2.5 < |y^*| < 4.0$.

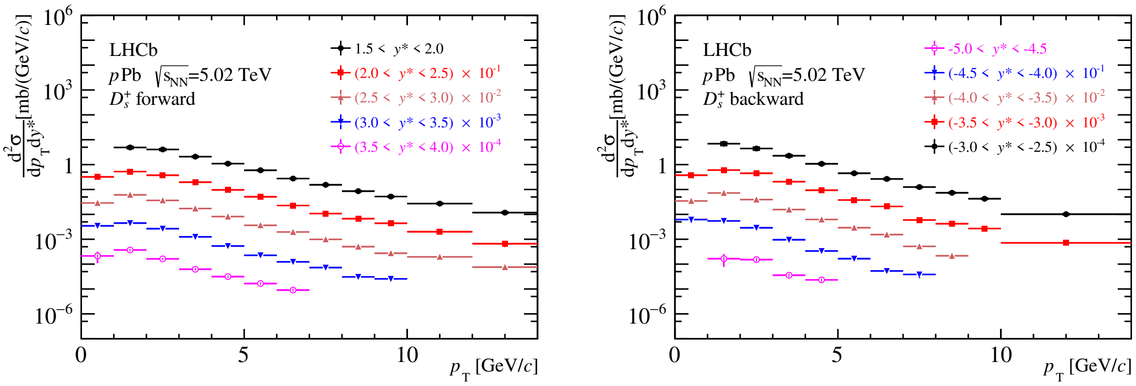

Figure 6. Double-differential cross-section of prompt D_s^+ mesons in pPb collisions for the (left) forward and (right) backward rapidities. The error bars are the statistical uncertainty and the boxes are the systematic uncertainty, both of which are smaller than the symbol size. The value in a particular rapidity interval is scaled by a multiplicative factor 10^{-m}, where the factor m increase as the rapidity rises.

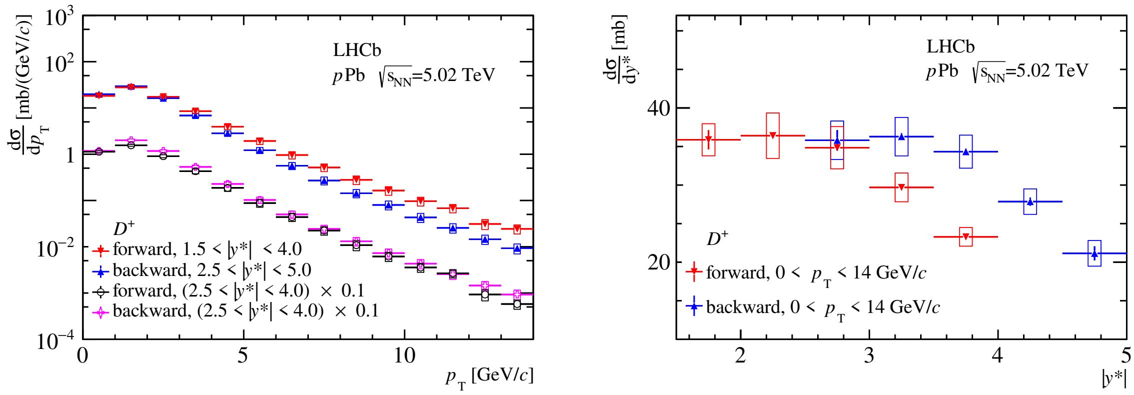

Figure 7. Differential cross-section of prompt D^+ meson production in pPb collisions as a function of (left) $p_{\rm T}$ and (right) y^* in the forward and backward collision samples. The error bars are the statistical uncertainty while the boxes are the systematic uncertainty.

The integrated production cross-sections of prompt D^+ and D_s^+ mesons in pPb forward collisions in the full and common fiducial regions are

$$
\begin{aligned}
\sigma(D^+)_{\rm forward}(0 < p_{\rm T} < 10\,{\rm GeV}/c, 1.5 < |y^*| < 4.0) &= 79.8 \pm 0.7 \pm 5.1\,{\rm mb},\\
\sigma(D^+)_{\rm forward}(0 < p_{\rm T} < 10\,{\rm GeV}/c, 2.5 < |y^*| < 4.0) &= 43.8 \pm 0.2 \pm 2.8\,{\rm mb},\\
\sigma(D_s^+)_{\rm forward}(1 < p_{\rm T} < 10\,{\rm GeV}/c, 1.5 < |y^*| < 4.0) &= 27.5 \pm 0.4 \pm 2.4\,{\rm mb},\\
\sigma(D_s^+)_{\rm forward}(1 < p_{\rm T} < 10\,{\rm GeV}/c, 2.5 < |y^*| < 4.0) &= 14.4 \pm 0.3 \pm 1.1\,{\rm mb}.
\end{aligned}
$$

The first uncertainties are statistical while the second are systematic. The integrated production cross-sections of prompt D^+ and D_s^+ mesons in pPb backward collisions in the

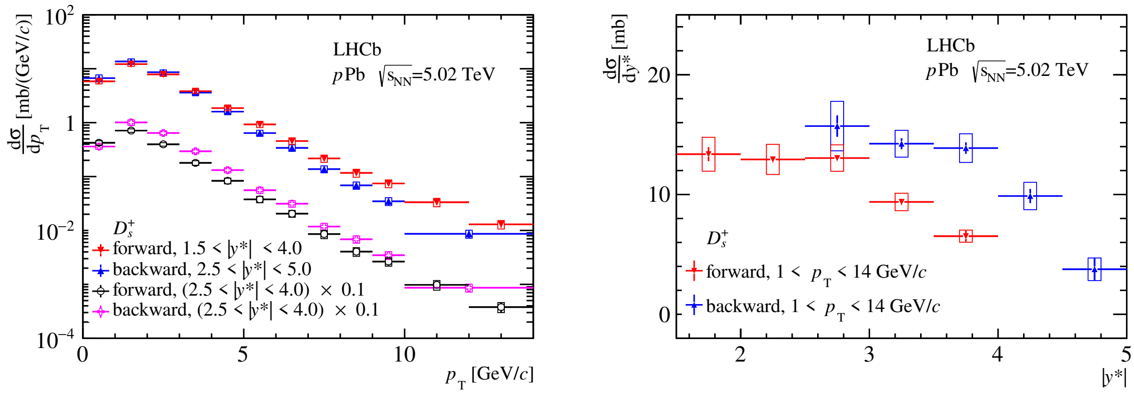

Figure 8. Differential cross-section of prompt D_s^+ meson production in pPb collisions as a function of (left) p_T and (right) y^* in the forward and backward collision samples. The error bars are the statistical uncertainty while the boxes are the systematic uncertainty.

full and common fiducial regions are

$$\sigma(D^+)_{\text{backward}}(0 < p_T < 10\,\text{GeV}/c, 2.5 < |y^*| < 5.0) = 77.6 \pm 0.9 \pm 4.9\,\text{mb},$$
$$\sigma(D^+)_{\text{backward}}(0 < p_T < 10\,\text{GeV}/c, 2.5 < |y^*| < 4.0) = 53.1 \pm 0.7 \pm 3.5\,\text{mb},$$
$$\sigma(D_s^+)_{\text{backward}}(1 < p_T < 10\,\text{GeV}/c, 2.5 < |y^*| < 5.0) = 28.7 \pm 0.8 \pm 3.0\,\text{mb},$$
$$\sigma(D_s^+)_{\text{backward}}(1 < p_T < 10\,\text{GeV}/c, 2.5 < |y^*| < 4.0) = 21.9 \pm 0.6 \pm 2.3\,\text{mb}.$$

5.2 Nuclear modification factors

The values of the D-meson production cross-section in pp collisions at 5.02 TeV, which are necessary for the measurement of the nuclear modification factor $R_{p\text{Pb}}$, are taken from ref. [53]. Systematic uncertainties associated with the hadronic interaction length and branching fractions of ref. [53] are fully correlated with the measurements presented here, while other uncertainties are assumed to be uncorrelated. The nuclear modification factors for prompt D^+ and D_s^+ production, displayed in figure 9 in bins of p_T and figure 10 in bins of y^*, show a slight increase as a function of p_T, implying that the suppression may decrease with increasing p_T. The values of $R_{p\text{Pb}}$ for D^+ and D_s^+ mesons are given in appendix B.

The measurements are compared with previous D^0 results by the LHCb collaboration at $\sqrt{s_{\text{NN}}} = 5.02$ TeV [36], as well as with the HELAC-Onia generator [76–78] using EPPS16 and nCTEQ15 nPDFs [79, 80], where the nPDFs are re-weighted with the D^0 cross-section [36]. At forward rapidity, the D^+ results agree very well with the $R_{p\text{Pb}}$ of D^0 mesons and the nPDF calculations within uncertainties. At backward rapidity, the D_s^+ results are consistent with the D^0 data and the nPDF calculations within uncertainties. However, the D^+ $R_{p\text{Pb}}$ seems to be systematically lower than D^0 and D_s^+ mesons across the whole p_T range due to the overall decrease in the R_{D^+/D^0} ratios at backward rapidity relative to the forward in figure 12. The D^+ $R_{p\text{Pb}}$ results at backward rapidity are lower than nPDF predictions with a significance of about $1-3$ standard deviations as further discussed in section 5.4, suggesting possible changes in charm hadronization in pPb collisions.

In figures 9 and 10 the measurements are also compared with predictions in the CGC framework, which include the effect of the saturation of partons at small Bjorken-x. For

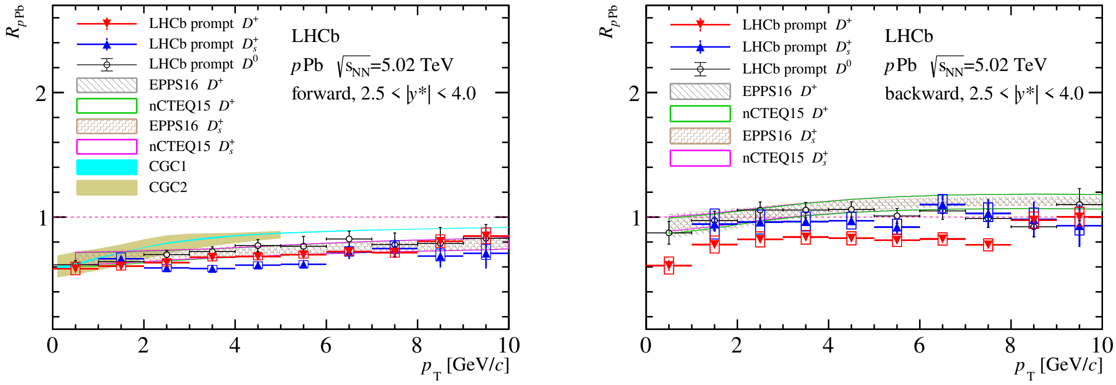

Figure 9. Nuclear modification factors $R_{p\mathrm{Pb}}$ as a function of p_T for prompt D^+ and D_s^+ meson production in the (left) forward data and (right) backward data. The error bars are the statistical uncertainty and the boxes are the systematic uncertainty. The CGC [73–75] predictions are only available in the forward region. Previous results on D^0 mesons [36] from LHCb are also shown.

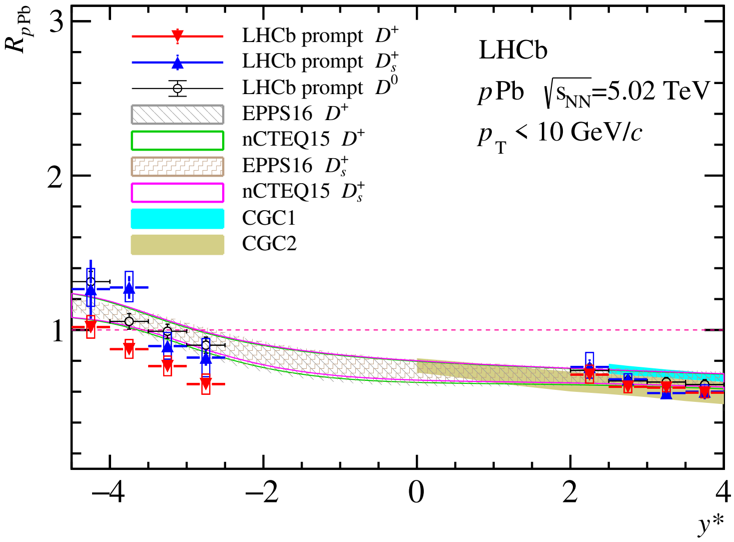

Figure 10. Nuclear modification factors $R_{p\mathrm{Pb}}$ as a function of y^* for prompt D^+ and D_s^+ meson production, integrated up to $p_\mathrm{T} = 10\,\mathrm{GeV}/c$. The error bars are the statistical uncertainty and the boxes are the systematic uncertainty. The CGC [73–75] predictions are only available in the forward region. Previous results on D^0 mesons [36] from LHCb are also shown.

CGC1 [73, 74], the cross-section of the D mesons is obtained with the optical Glauber mechanism correlating the initial state of the nucleon with that of the proton, and for CGC2 [75], it is derived by convolving the charm-quark fragmentation function in a transverse momentum-dependent factorization framework. The CGC models are found to be able to describe the trend of prompt D-meson nuclear modifications as a function of p_T and of rapidity in the forward regions.

5.3 Forward-backward ratio

In the forward-backward production ratio R_{FB}, the uncertainties from common sources between the forward and backward measurements cancel out. The uncertainties due to branching fractions and to hadronic interactions with the detector are considered fully correlated, while other uncertainties are conservatively treated as uncorrelated. The measured R_{FB} values for D^+ and D_s^+ mesons are shown in figure 11, as a function of p_{T} integrated over the range $2.5 < |y^*| < 4.0$, and as a function of y^* integrated up to $p_{\mathrm{T}} = 14\,\mathrm{GeV}/c$. The R_{FB} values in different kinematic bins are tabulated in appendix C. The R_{FB} values for D^+ and D_s^+ mesons are also compared to the measurements of D^0 mesons [36] and Λ_c^+ baryons [37] by the LHCb collaboration at $\sqrt{s_{\mathrm{NN}}} = 5.02\,\mathrm{TeV}$ in figure 11. The R_{FB} of all open charm hadrons deviates further from unity as $|y^*|$ increases. This behavior is consistent with the expectations from the QCD calculations, suggesting that the asymmetry becomes more pronounced in the large rapidity region. The R_{FB} of D_s^+ mesons as a function of y^* shows reasonable agreement with D^0 and Λ_c^+ results and with the EPPS16 and nCTEQ15 nPDFs [79, 80] within uncertainties. The R_{FB} of D^+ mesons as a function of y^* is slightly larger than other charm hadrons and model predictions. At low p_{T}, the R_{FB} of D^+ and D_s^+ mesons are consistent with the R_{FB} of D^0 mesons and Λ_c^+ baryons, and agree with nPDFs calculations. However, the more precise D^+ data show a clear increasing trend with increasing p_{T} and saturates at unity at high p_{T} ($> 10\,\mathrm{GeV}/c$) within uncertainties, which deviates from the almost p_{T} independent nPDF calculations. This discrepancy derives from the overall suppression of D^+ production as a function of p_{T} in the backward configuration, which is also pronounced in figure 9.

5.4 Production ratios

The measured prompt D_s^+ and D^+ production cross-sections enable a calculation of D_s^+ to D^+ ratios. The LHCb measurement of D^0 cross-sections in pPb collisions at $\sqrt{s_{\mathrm{NN}}} = 5.02\,\mathrm{TeV}$ [36] also enables a calculation of the ratio of the production cross-sections of D^+ to D^0 and D_s^+ to D^0 mesons. The uncertainty due to hadronic interactions with the detector is considered partially correlated because of different numbers of kaon and pion tracks between the numerators and denominators of R_{D^+/D^0}, $R_{D_s^+/D^0}$ or $R_{D_s^+/D^+}$. The uncertainties from the luminosity are fully correlated, while the remaining uncertainties are uncorrelated. Figure 12 illustrates the R_{D^+/D^0}, $R_{D_s^+/D^0}$ and $R_{D_s^+/D^+}$ ratios as a function of p_{T} integrated over total rapidity range $1.5 < y^* < 4.0$ for forward and $-5.0 < y^* < -2.5$ for backward. Figure 13 illustrates the R_{D^+/D^0}, $R_{D_s^+/D^0}$ and $R_{D_s^+/D^+}$ ratios as a function of y^* integrated over the p_{T} range up to $10\,\mathrm{GeV}/c$. The measured production ratios are tabulated in appendix D.

The results of relative cross-section ratios between D mesons in LHCb pPb collisions show a mild p_{T} and y^* dependence, which are consistent with the results from the LHCb collaboration in pp [53], and from the ALICE collaboration in pPb [38] and in pp [15] collisions. The $R_{D_s^+/D^0}$ and $R_{D_s^+/D^+}$ ratios are found not to be enhanced in neither forward nor backward rapidities in pPb collisions at $\sqrt{s_{\mathrm{NN}}} = 5.02\,\mathrm{TeV}$. The lower R_{D^+/D^0} ratios at backward rapidity relative to the forward region lead to differences in the results of $R_{p\mathrm{Pb}}$ and R_{FB} for D^+ versus other D mesons. On average, the multiplicity value at backward rapidity is 1.6 times higher than that at forward rapidity in terms of the backward-forward production ratio of charged particles at the same center-of-mass energy from LHCb [81].

JHEP01(2024)070

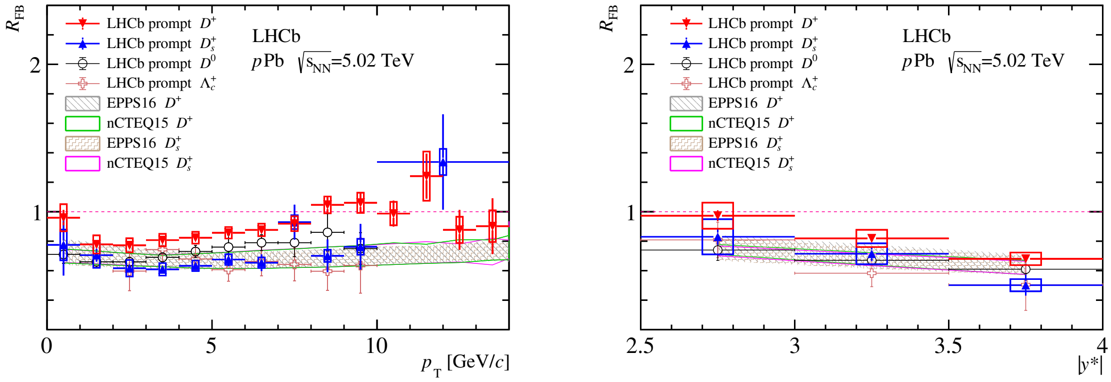

Figure 11. Forward-backward ratios $R_{\rm FB}$ for prompt D^+ and D_s^+ meson production (left) as a function of $p_{\rm T}$; (right) as a function of y^*. The error bars are the statistical uncertainty while the boxes are the systematic uncertainty. Previous results on D^0 [36] mesons and Λ_c^+ [37] baryons from LHCb are also shown.

As some contributions of D^+ and D^0 mesons come from the decay of the excited charm resonance, the D^{*+} meson [65, 82], it may be possible to further understand this phenomenon by investigating the production of D^{*+} mesons in high multiplicity pPb events.

6 Conclusion

The prompt D^+ and D_s^+ production cross-sections have been measured with LHCb proton-lead collision data corresponding to an integrated luminosity of $(1.58 \pm 0.02)\,\mathrm{nb}^{-1}$ collected at $\sqrt{s_{\rm NN}} = 5.02\,\mathrm{TeV}$. The measurement is performed in the range of the D-meson transverse momentum $0 < p_{\rm T} < 14\,\mathrm{GeV}/c$, in both backward and forward collisions covering the rapidity ranges $1.5 < y^* < 4.0$ and $-5.0 < y^* < -2.5$. This is the first measurement in this rapidity region down to zero transverse momentum of the D^+ and D_s^+ mesons. Nuclear modification factors and forward-backward production ratios are also measured in the same kinematic region. A large asymmetry in the forward-backward production is observed, which is consistent with the expectations from nuclear parton distribution functions, and colour glass condensate calculations. The $R_{D_s^+/D^0}$ and $R_{D_s^+/D^+}$ ratios show no enhancement of the yield of strange hadrons at high transverse momentum or rapidity, and may therefore be used as a reference for experimental measurements related to investigations of the QGP in nucleus-nucleus collisions.

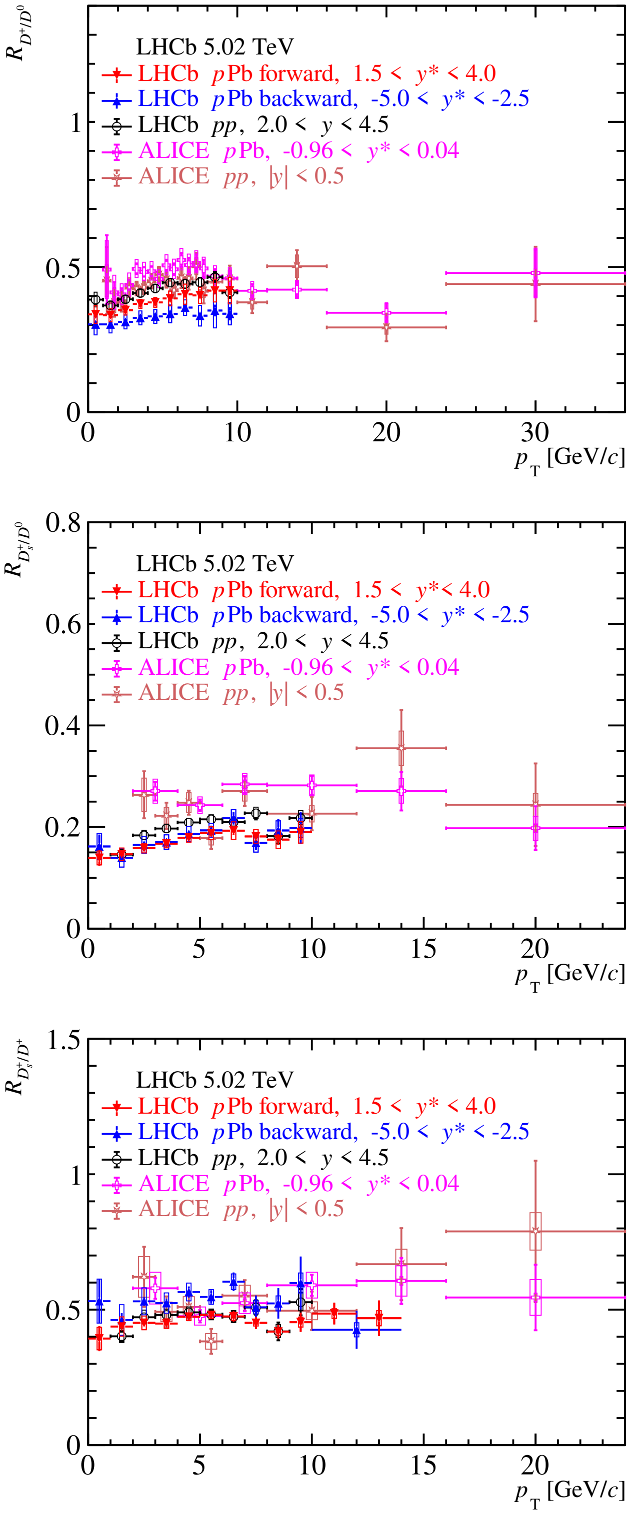

Figure 12. Production ratios as a function of p_{T} in LHCb pPb collisions. The error bars show the statistical uncertainty while the boxes show the systematic uncertainty. The uncertainties related to the branching fractions are not shown in the figure. The measurements are also compared with other results of pp [15, 53] and pPb [38] collisions at the same centre-of-mass energy from LHCb and ALICE.

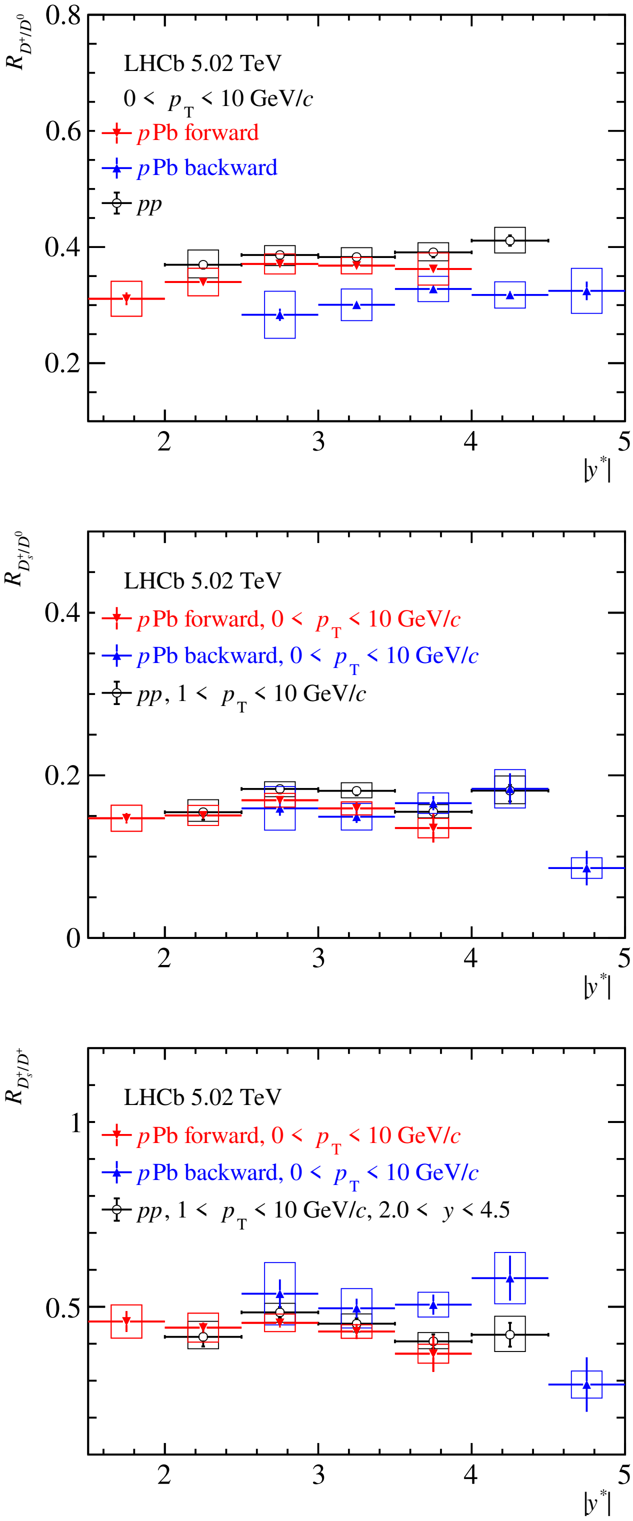

Figure 13. Production ratios as a function of y^* in LHCb pPb collisions. The error bars show the statistical uncertainty while the boxes show the systematic uncertainty. The uncertainties related to the branching fractions are not shown in the figure. The measurements are also compared with the results of pp collisions at the same centre-of-mass energy from LHCb [53].

Acknowledgments

We express our gratitude to our colleagues in the CERN accelerator departments for the excellent performance of the LHC. We thank the technical and administrative staff at the LHCb institutes. We acknowledge support from CERN and from the national agencies: CAPES, CNPq, FAPERJ and FINEP (Brazil); MOST and NSFC (China); CNRS/IN2P3 (France); BMBF, DFG and MPG (Germany); INFN (Italy); NWO (Netherlands); MNiSW and NCN (Poland); MCID/IFA (Romania); MICINN (Spain); SNSF and SER (Switzerland); NASU (Ukraine); STFC (United Kingdom); DOE NP and NSF (U.S.A.). We acknowledge the computing resources that are provided by CERN, IN2P3 (France), KIT and DESY (Germany), INFN (Italy), SURF (Netherlands), PIC (Spain), GridPP (United Kingdom), CSCS (Switzerland), IFIN-HH (Romania), CBPF (Brazil), Polish WLCG (Poland) and NERSC (U.S.A.). We are indebted to the communities behind the multiple open-source software packages on which we depend. Individual groups or members have received support from ARC and ARDC (Australia); Minciencias (Colombia); AvH Foundation (Germany); EPLANET, Marie Skłodowska-Curie Actions, ERC and NextGenerationEU (European Union); A*MIDEX, ANR, IPhU and Labex P2IO, and Région Auvergne-Rhône-Alpes (France); Key Research Program of Frontier Sciences of CAS, CAS PIFI, CAS CCEPP, Fundamental Research Funds for the Central Universities, and Sci. & Tech. Program of Guangzhou (China); GVA, XuntaGal, GENCAT, Inditex, InTalent and Prog. Atracción Talento, CM (Spain); SRC (Sweden); the Leverhulme Trust, the Royal Society and UKRI (United Kingdom).

A Numerical values of the D^+ and D_s^+ mesons cross-sections

Tables 2–5 give the numerical results for the double-differential cross-sections. Tables 6–11 give the numerical results for the one-dimensional differential cross-sections.

Forward					
p_{T} [GeV/c]	$1.5 < y^* < 2.0$	$2.0 < y^* < 2.5$	$2.5 < y^* < 3.0$	$3.0 < y^* < 3.5$	$3.5 < y^* < 4.0$
$[0, 1]$	$6.835 \pm 1.131 \pm 0.590 \pm 0.528$	$7.069 \pm 0.207 \pm 0.104 \pm 0.766$	$7.953 \pm 0.164 \pm 0.085 \pm 0.659$	$7.527 \pm 0.185 \pm 0.091 \pm 0.393$	$7.132 \pm 0.270 \pm 0.134 \pm 0.468$
$[1, 2]$	$11.748 \pm 0.481 \pm 0.282 \pm 0.848$	$12.768 \pm 0.157 \pm 0.092 \pm 1.079$	$12.198 \pm 0.122 \pm 0.069 \pm 0.806$	$10.733 \pm 0.130 \pm 0.071 \pm 0.609$	$8.238 \pm 0.187 \pm 0.091 \pm 0.487$
$[2, 3]$	$8.377 \pm 0.165 \pm 0.102 \pm 0.527$	$8.348 \pm 0.067 \pm 0.041 \pm 0.671$	$7.552 \pm 0.054 \pm 0.032 \pm 0.704$	$6.096 \pm 0.054 \pm 0.034 \pm 0.523$	$4.476 \pm 0.075 \pm 0.039 \pm 0.307$
$[3, 4]$	$4.383 \pm 0.069 \pm 0.044 \pm 0.274$	$4.067 \pm 0.032 \pm 0.018 \pm 0.500$	$3.678 \pm 0.027 \pm 0.016 \pm 0.539$	$2.873 \pm 0.027 \pm 0.015 \pm 0.379$	$2.040 \pm 0.037 \pm 0.019 \pm 0.178$
$[4, 5]$	$2.103 \pm 0.034 \pm 0.020 \pm 0.156$	$2.015 \pm 0.018 \pm 0.010 \pm 0.338$	$1.704 \pm 0.016 \pm 0.009 \pm 0.321$	$1.238 \pm 0.015 \pm 0.008 \pm 0.216$	$0.805 \pm 0.021 \pm 0.009 \pm 0.081$
$[5, 6]$	$1.108 \pm 0.020 \pm 0.012 \pm 0.099$	$0.999 \pm 0.012 \pm 0.006 \pm 0.204$	$0.808 \pm 0.010 \pm 0.005 \pm 0.183$	$0.601 \pm 0.010 \pm 0.005 \pm 0.124$	$0.348 \pm 0.015 \pm 0.006 \pm 0.033$
$[6, 7]$	$0.550 \pm 0.012 \pm 0.007 \pm 0.059$	$0.494 \pm 0.008 \pm 0.004 \pm 0.115$	$0.412 \pm 0.007 \pm 0.003 \pm 0.103$	$0.294 \pm 0.007 \pm 0.003 \pm 0.064$	$0.170 \pm 0.013 \pm 0.005 \pm 0.017$
$[7, 8]$	$0.318 \pm 0.009 \pm 0.005 \pm 0.038$	$0.267 \pm 0.005 \pm 0.003 \pm 0.067$	$0.231 \pm 0.005 \pm 0.002 \pm 0.061$	$0.144 \pm 0.005 \pm 0.002 \pm 0.030$	$0.073 \pm 0.015 \pm 0.005 \pm 0.009$
$[8, 9]$	$0.188 \pm 0.006 \pm 0.004 \pm 0.025$	$0.154 \pm 0.004 \pm 0.002 \pm 0.041$	$0.133 \pm 0.004 \pm 0.002 \pm 0.037$	$0.084 \pm 0.004 \pm 0.002 \pm 0.016$	—
$[9, 10]$	$0.111 \pm 0.005 \pm 0.002 \pm 0.017$	$0.094 \pm 0.003 \pm 0.001 \pm 0.026$	$0.072 \pm 0.003 \pm 0.001 \pm 0.021$	$0.052 \pm 0.004 \pm 0.002 \pm 0.008$	—
$[10, 11]$	$0.066 \pm 0.003 \pm 0.002 \pm 0.011$	$0.056 \pm 0.002 \pm 0.001 \pm 0.016$	$0.043 \pm 0.002 \pm 0.001 \pm 0.012$	$0.028 \pm 0.004 \pm 0.002 \pm 0.004$	—
$[11, 12]$	$0.043 \pm 0.003 \pm 0.001 \pm 0.007$	$0.040 \pm 0.002 \pm 0.001 \pm 0.011$	$0.027 \pm 0.002 \pm 0.001 \pm 0.007$	$0.026 \pm 0.004 \pm 0.003 \pm 0.005$	—
$[12, 13]$	$0.022 \pm 0.002 \pm 0.001 \pm 0.004$	$0.022 \pm 0.002 \pm 0.001 \pm 0.007$	$0.019 \pm 0.002 \pm 0.001 \pm 0.005$	—	—
$[13, 14]$	$0.023 \pm 0.002 \pm 0.001 \pm 0.004$	$0.014 \pm 0.001 \pm 0.001 \pm 0.004$	$0.012 \pm 0.001 \pm 0.001 \pm 0.003$	—	—

Table 2. Double-differential cross-section (mb) for prompt D^+ mesons as functions of p_{T} and y^* in the forward regions. The first uncertainty is statistical, the second is the component of the systematic uncertainty that is uncorrelated between bins and the third is the fully correlated component.

Backward					
p_{T} [GeV/c]	$-3.0 < y^* < -2.5$	$-3.5 < y^* < -3.0$	$-4.0 < y^* < -3.5$	$-4.5 < y^* < -4.0$	$-5.0 < y^* < -4.5$
$[0, 1]$	$6.430 \pm 1.127 \pm 0.371 \pm 0.647$	$7.921 \pm 0.340 \pm 0.115 \pm 0.835$	$9.220 \pm 0.321 \pm 0.106 \pm 0.607$	$8.069 \pm 0.438 \pm 0.115 \pm 0.571$	$8.054 \pm 0.750 \pm 0.195 \pm 0.715$
$[1, 2]$	$13.372 \pm 0.641 \pm 0.321 \pm 0.966$	$13.751 \pm 0.252 \pm 0.099 \pm 1.162$	$12.931 \pm 0.221 \pm 0.073 \pm 0.855$	$11.049 \pm 0.283 \pm 0.073 \pm 0.627$	$7.973 \pm 0.497 \pm 0.088 \pm 0.471$
$[2, 3]$	$8.325 \pm 0.210 \pm 0.101 \pm 0.524$	$8.064 \pm 0.102 \pm 0.040 \pm 0.649$	$7.087 \pm 0.087 \pm 0.030 \pm 0.661$	$5.434 \pm 0.092 \pm 0.030 \pm 0.467$	$3.603 \pm 0.138 \pm 0.032 \pm 0.247$
$[3, 4]$	$4.058 \pm 0.086 \pm 0.040 \pm 0.254$	$3.616 \pm 0.046 \pm 0.016 \pm 0.445$	$2.965 \pm 0.039 \pm 0.013 \pm 0.435$	$2.017 \pm 0.038 \pm 0.011 \pm 0.266$	$1.081 \pm 0.052 \pm 0.010 \pm 0.094$
$[4, 5]$	$1.824 \pm 0.042 \pm 0.018 \pm 0.135$	$1.533 \pm 0.024 \pm 0.008 \pm 0.257$	$1.194 \pm 0.021 \pm 0.006 \pm 0.225$	$0.775 \pm 0.020 \pm 0.005 \pm 0.135$	$0.338 \pm 0.026 \pm 0.004 \pm 0.034$
$[5, 6]$	$0.857 \pm 0.024 \pm 0.009 \pm 0.077$	$0.702 \pm 0.015 \pm 0.004 \pm 0.144$	$0.492 \pm 0.012 \pm 0.003 \pm 0.111$	$0.294 \pm 0.011 \pm 0.002 \pm 0.060$	$0.094 \pm 0.017 \pm 0.002 \pm 0.009$
$[6, 7]$	$0.433 \pm 0.015 \pm 0.006 \pm 0.046$	$0.340 \pm 0.009 \pm 0.003 \pm 0.079$	$0.227 \pm 0.008 \pm 0.002 \pm 0.057$	$0.128 \pm 0.008 \pm 0.001 \pm 0.028$	—
$[7, 8]$	$0.223 \pm 0.009 \pm 0.003 \pm 0.026$	$0.159 \pm 0.006 \pm 0.002 \pm 0.040$	$0.106 \pm 0.005 \pm 0.001 \pm 0.028$	$0.053 \pm 0.005 \pm 0.001 \pm 0.011$	—
$[8, 9]$	$0.120 \pm 0.007 \pm 0.002 \pm 0.016$	$0.087 \pm 0.004 \pm 0.001 \pm 0.023$	$0.055 \pm 0.004 \pm 0.001 \pm 0.015$	$0.024 \pm 0.004 \pm 0.001 \pm 0.005$	—
$[9, 10]$	$0.065 \pm 0.005 \pm 0.001 \pm 0.010$	$0.051 \pm 0.003 \pm 0.001 \pm 0.014$	$0.030 \pm 0.003 \pm 0.001 \pm 0.009$	$0.014 \pm 0.004 \pm 0.001 \pm 0.002$	—
$[10, 11]$	$0.042 \pm 0.004 \pm 0.001 \pm 0.007$	$0.030 \pm 0.003 \pm 0.001 \pm 0.009$	$0.014 \pm 0.002 \pm 0.000 \pm 0.004$	—	—
$[11, 12]$	$0.029 \pm 0.003 \pm 0.001 \pm 0.005$	$0.014 \pm 0.002 \pm 0.000 \pm 0.004$	$0.008 \pm 0.001 \pm 0.000 \pm 0.002$	—	—
$[12, 13]$	$0.021 \pm 0.002 \pm 0.001 \pm 0.004$	$0.008 \pm 0.001 \pm 0.000 \pm 0.002$	—	—	—
$[13, 14]$	$0.013 \pm 0.002 \pm 0.001 \pm 0.002$	$0.006 \pm 0.001 \pm 0.000 \pm 0.002$	—	—	—

Table 3. Double-differential cross-section (mb) for prompt D^+ mesons as functions of p_{T} and y^* in the backward regions. The first uncertainty is statistical, the second is the component of the systematic uncertainty that is uncorrelated between bins and the third is the fully correlated component.

Forward					
$p_{\mathrm{T}}\,[\mathrm{GeV}/c]$	$1.5 < y^* < 2.0$	$2.0 < y^* < 2.5$	$2.5 < y^* < 3.0$	$3.0 < y^* < 3.5$	$3.5 < y^* < 4.0$
$[0, 1]$	—	$3.213 \pm 0.403 \pm 0.123 \pm 0.441$	$2.873 \pm 0.346 \pm 0.097 \pm 0.317$	$3.454 \pm 0.538 \pm 0.147 \pm 0.303$	$2.134 \pm 1.045 \pm 0.175 \pm 0.205$
$[1, 2]$	$4.885 \pm 0.521 \pm 0.170 \pm 0.621$	$5.250 \pm 0.227 \pm 0.073 \pm 0.602$	$6.079 \pm 0.219 \pm 0.077 \pm 0.505$	$4.464 \pm 0.235 \pm 0.072 \pm 0.356$	$3.699 \pm 0.415 \pm 0.110 \pm 0.316$
$[2, 3]$	$4.059 \pm 0.221 \pm 0.078 \pm 0.487$	$3.738 \pm 0.104 \pm 0.034 \pm 0.356$	$3.640 \pm 0.094 \pm 0.034 \pm 0.318$	$2.659 \pm 0.098 \pm 0.033 \pm 0.217$	$1.630 \pm 0.149 \pm 0.038 \pm 0.133$
$[3, 4]$	$2.090 \pm 0.093 \pm 0.031 \pm 0.211$	$1.967 \pm 0.052 \pm 0.018 \pm 0.218$	$1.717 \pm 0.046 \pm 0.017 \pm 0.199$	$1.248 \pm 0.046 \pm 0.016 \pm 0.130$	$0.623 \pm 0.065 \pm 0.016 \pm 0.054$
$[4, 5]$	$1.096 \pm 0.051 \pm 0.017 \pm 0.101$	$0.964 \pm 0.030 \pm 0.010 \pm 0.133$	$0.817 \pm 0.027 \pm 0.009 \pm 0.118$	$0.534 \pm 0.026 \pm 0.008 \pm 0.069$	$0.315 \pm 0.035 \pm 0.008 \pm 0.029$
$[5, 6]$	$0.592 \pm 0.032 \pm 0.011 \pm 0.058$	$0.509 \pm 0.020 \pm 0.006 \pm 0.081$	$0.363 \pm 0.017 \pm 0.006 \pm 0.059$	$0.226 \pm 0.016 \pm 0.004 \pm 0.034$	$0.166 \pm 0.029 \pm 0.006 \pm 0.016$
$[6, 7]$	$0.275 \pm 0.019 \pm 0.007 \pm 0.029$	$0.227 \pm 0.012 \pm 0.004 \pm 0.040$	$0.196 \pm 0.012 \pm 0.004 \pm 0.035$	$0.124 \pm 0.011 \pm 0.003 \pm 0.020$	$0.090 \pm 0.022 \pm 0.005 \pm 0.009$
$[7, 8]$	$0.154 \pm 0.013 \pm 0.004 \pm 0.018$	$0.108 \pm 0.008 \pm 0.002 \pm 0.020$	$0.099 \pm 0.008 \pm 0.002 \pm 0.019$	$0.073 \pm 0.009 \pm 0.002 \pm 0.012$	—
$[8, 9]$	$0.086 \pm 0.009 \pm 0.003 \pm 0.011$	$0.067 \pm 0.006 \pm 0.002 \pm 0.014$	$0.050 \pm 0.006 \pm 0.001 \pm 0.010$	$0.031 \pm 0.006 \pm 0.001 \pm 0.005$	—
$[9, 10]$	$0.052 \pm 0.007 \pm 0.002 \pm 0.007$	$0.044 \pm 0.005 \pm 0.001 \pm 0.009$	$0.027 \pm 0.004 \pm 0.001 \pm 0.006$	$0.026 \pm 0.006 \pm 0.002 \pm 0.004$	—
$[10, 12]$	$0.027 \pm 0.004 \pm 0.001 \pm 0.004$	$0.020 \pm 0.002 \pm 0.001 \pm 0.004$	$0.020 \pm 0.002 \pm 0.001 \pm 0.004$	—	—
$[12, 14]$	$0.012 \pm 0.002 \pm 0.001 \pm 0.002$	$0.007 \pm 0.002 \pm 0.000 \pm 0.001$	$0.008 \pm 0.002 \pm 0.000 \pm 0.002$	—	—

Table 4. Double-differential cross-section (mb) for prompt D_s^+ mesons as functions of p_{T} and y^* in the forward regions. The first uncertainty is statistical, the second is the component of the systematic uncertainty that is uncorrelated between bins and the third is the fully correlated component.

Backward					
$p_{\mathrm{T}}\,[\mathrm{GeV}/c]$	$-3.0 < y^* < -2.5$	$-3.5 < y^* < -3.0$	$-4.0 < y^* < -3.5$	$-4.5 < y^* < -4.0$	$-5.0 < y^* < -4.5$
$[0, 1]$	—	$3.749 \pm 0.796 \pm 0.164 \pm 0.556$	$3.461 \pm 0.780 \pm 0.127 \pm 0.351$	$6.190 \pm 1.561 \pm 0.314 \pm 1.169$	—
$[1, 2]$	$6.929 \pm 0.818 \pm 0.212 \pm 1.243$	$6.020 \pm 0.400 \pm 0.086 \pm 0.777$	$7.245 \pm 0.440 \pm 0.103 \pm 0.655$	$5.443 \pm 0.549 \pm 0.107 \pm 0.678$	$1.654 \pm 0.877 \pm 0.129 \pm 0.202$
$[2, 3]$	$4.441 \pm 0.305 \pm 0.075 \pm 0.723$	$4.488 \pm 0.181 \pm 0.044 \pm 0.469$	$3.931 \pm 0.157 \pm 0.039 \pm 0.369$	$2.883 \pm 0.182 \pm 0.044 \pm 0.268$	$1.519 \pm 0.265 \pm 0.050 \pm 0.205$
$[3, 4]$	$2.270 \pm 0.137 \pm 0.032 \pm 0.293$	$2.062 \pm 0.082 \pm 0.019 \pm 0.235$	$1.559 \pm 0.068 \pm 0.016 \pm 0.182$	$0.955 \pm 0.065 \pm 0.014 \pm 0.101$	$0.358 \pm 0.093 \pm 0.014 \pm 0.043$
$[4, 5]$	$1.077 \pm 0.070 \pm 0.017 \pm 0.116$	$0.934 \pm 0.045 \pm 0.011 \pm 0.127$	$0.622 \pm 0.036 \pm 0.008 \pm 0.087$	$0.337 \pm 0.034 \pm 0.007 \pm 0.042$	$0.232 \pm 0.053 \pm 0.011 \pm 0.027$
$[5, 6]$	$0.450 \pm 0.037 \pm 0.008 \pm 0.051$	$0.377 \pm 0.025 \pm 0.005 \pm 0.059$	$0.290 \pm 0.022 \pm 0.005 \pm 0.046$	$0.166 \pm 0.020 \pm 0.004 \pm 0.024$	—
$[6, 7]$	$0.265 \pm 0.026 \pm 0.006 \pm 0.032$	$0.208 \pm 0.017 \pm 0.004 \pm 0.036$	$0.154 \pm 0.015 \pm 0.004 \pm 0.025$	$0.053 \pm 0.011 \pm 0.002 \pm 0.008$	—
$[7, 8]$	$0.125 \pm 0.015 \pm 0.003 \pm 0.017$	$0.059 \pm 0.008 \pm 0.001 \pm 0.011$	$0.052 \pm 0.009 \pm 0.002 \pm 0.009$	$0.038 \pm 0.011 \pm 0.002 \pm 0.006$	—
$[8, 9]$	$0.074 \pm 0.010 \pm 0.003 \pm 0.010$	$0.042 \pm 0.008 \pm 0.001 \pm 0.008$	$0.022 \pm 0.006 \pm 0.001 \pm 0.004$	—	—
$[9, 10]$	$0.043 \pm 0.009 \pm 0.002 \pm 0.007$	$0.027 \pm 0.005 \pm 0.001 \pm 0.005$	—	—	—
$[10, 14]$	$0.010 \pm 0.002 \pm 0.000 \pm 0.002$	$0.007 \pm 0.001 \pm 0.000 \pm 0.002$	—	—	—

Table 5. Double-differential cross-section (mb) for prompt D_s^+ mesons as functions of p_{T} and y^* in the backward regions. The first uncertainty is statistical, the second is the component of the systematic uncertainty that is uncorrelated between bins and the third is the fully correlated component.

Forward

$p_{\mathrm{T}}\,[\mathrm{GeV}/c]$	y^*	$\frac{\mathrm{d}\sigma}{\mathrm{d}p_{\mathrm{T}}}\;[\mathrm{mb}/(\mathrm{GeV}/c)]$
$[0, 1]$	$[1.5, 4.0]$	$18.258 \pm 0.603 \pm 0.313 \pm 1.180$
$[1, 2]$	$[1.5, 4.0]$	$27.842 \pm 0.284 \pm 0.163 \pm 1.510$
$[2, 3]$	$[1.5, 4.0]$	$17.424 \pm 0.104 \pm 0.063 \pm 1.103$
$[3, 4]$	$[1.5, 4.0]$	$8.521 \pm 0.047 \pm 0.028 \pm 0.840$
$[4, 5]$	$[1.5, 4.0]$	$3.933 \pm 0.025 \pm 0.014 \pm 0.526$
$[5, 6]$	$[1.5, 4.0]$	$1.932 \pm 0.015 \pm 0.008 \pm 0.310$
$[6, 7]$	$[1.5, 4.0]$	$0.960 \pm 0.011 \pm 0.005 \pm 0.171$
$[7, 8]$	$[1.5, 4.0]$	$0.517 \pm 0.010 \pm 0.004 \pm 0.097$
$[8, 9]$	$[1.5, 3.5]$	$0.279 \pm 0.005 \pm 0.002 \pm 0.059$
$[9, 10]$	$[1.5, 3.5]$	$0.164 \pm 0.004 \pm 0.002 \pm 0.034$
$[10, 11]$	$[1.5, 3.5]$	$0.097 \pm 0.003 \pm 0.001 \pm 0.021$
$[11, 12]$	$[1.5, 3.5]$	$0.068 \pm 0.003 \pm 0.002 \pm 0.014$
$[12, 13]$	$[1.5, 3.0]$	$0.031 \pm 0.001 \pm 0.001 \pm 0.008$
$[13, 14]$	$[1.5, 3.0]$	$0.024 \pm 0.001 \pm 0.001 \pm 0.005$

Backward

$p_{\mathrm{T}}\,[\mathrm{GeV}/c]$	y^*	$\frac{\mathrm{d}\sigma}{\mathrm{d}p_{\mathrm{T}}}\;[\mathrm{mb}/(\mathrm{GeV}/c)]$
$[0, 1]$	$[-5.0, -2.5]$	$19.847 \pm 0.749 \pm 0.231 \pm 1.276$
$[1, 2]$	$[-5.0, -2.5]$	$29.538 \pm 0.461 \pm 0.169 \pm 1.705$
$[2, 3]$	$[-5.0, -2.5]$	$16.257 \pm 0.150 \pm 0.058 \pm 1.070$
$[3, 4]$	$[-5.0, -2.5]$	$6.869 \pm 0.062 \pm 0.024 \pm 0.663$
$[4, 5]$	$[-5.0, -2.5]$	$2.832 \pm 0.031 \pm 0.011 \pm 0.365$
$[5, 6]$	$[-5.0, -2.5]$	$1.219 \pm 0.018 \pm 0.006 \pm 0.187$
$[6, 7]$	$[-4.5, -2.5]$	$0.564 \pm 0.010 \pm 0.004 \pm 0.100$
$[7, 8]$	$[-4.5, -2.5]$	$0.270 \pm 0.007 \pm 0.002 \pm 0.052$
$[8, 9]$	$[-4.5, -2.5]$	$0.143 \pm 0.005 \pm 0.002 \pm 0.029$
$[9, 10]$	$[-4.5, -2.5]$	$0.080 \pm 0.004 \pm 0.001 \pm 0.017$
$[10, 11]$	$[-4.0, -2.5]$	$0.043 \pm 0.002 \pm 0.001 \pm 0.010$
$[11, 12]$	$[-4.0, -2.5]$	$0.026 \pm 0.002 \pm 0.001 \pm 0.006$
$[12, 13]$	$[-3.5, -2.5]$	$0.015 \pm 0.001 \pm 0.000 \pm 0.003$
$[13, 14]$	$[-3.5, -2.5]$	$0.009 \pm 0.001 \pm 0.000 \pm 0.002$

Table 6. Differential cross-section for prompt D^+ mesons as a function of p_{T} in the total forward and backward rapidity regions, respectively. The first uncertainty is statistical, the second is the component of the systematic uncertainty that is uncorrelated between bins and the third is the fully correlated component.

Forward

$p_{\mathrm{T}}\,[\,\mathrm{GeV}/c]$	y^*	$\frac{\mathrm{d}\sigma}{\mathrm{d}p_{\mathrm{T}}}\ [\,\mathrm{mb}/(\,\mathrm{GeV}/c)]$
$[0, 1]$	$[2.0, 4.0]$	$5.837 \pm 0.645 \pm 0.139 \pm 0.591$
$[1, 2]$	$[1.5, 4.0]$	$12.189 \pm 0.387 \pm 0.120 \pm 1.087$
$[2, 3]$	$[1.5, 4.0]$	$7.864 \pm 0.158 \pm 0.052 \pm 0.649$
$[3, 4]$	$[1.5, 4.0]$	$3.823 \pm 0.070 \pm 0.023 \pm 0.360$
$[4, 5]$	$[1.5, 4.0]$	$1.863 \pm 0.039 \pm 0.012 \pm 0.209$
$[5, 6]$	$[1.5, 4.0]$	$0.928 \pm 0.026 \pm 0.008 \pm 0.117$
$[6, 7]$	$[1.5, 4.0]$	$0.456 \pm 0.018 \pm 0.005 \pm 0.063$
$[7, 8]$	$[1.5, 3.5]$	$0.217 \pm 0.010 \pm 0.003 \pm 0.033$
$[8, 9]$	$[1.5, 3.5]$	$0.117 \pm 0.007 \pm 0.002 \pm 0.019$
$[9, 10]$	$[1.5, 3.5]$	$0.074 \pm 0.006 \pm 0.002 \pm 0.012$
$[10, 12]$	$[1.5, 3.0]$	$0.033 \pm 0.002 \pm 0.001 \pm 0.006$
$[12, 14]$	$[1.5, 3.0]$	$0.013 \pm 0.002 \pm 0.000 \pm 0.002$

Backward

$p_{\mathrm{T}}\,[\,\mathrm{GeV}/c]$	y^*	$\frac{\mathrm{d}\sigma}{\mathrm{d}p_{\mathrm{T}}}\ [\,\mathrm{mb}/(\,\mathrm{GeV}/c)]$
$[0, 1]$	$[-4.5, -3.0]$	$6.700 \pm 0.959 \pm 0.188 \pm 0.966$
$[1, 2]$	$[-5.0, -2.5]$	$13.646 \pm 0.723 \pm 0.151 \pm 1.587$
$[2, 3]$	$[-5.0, -2.5]$	$8.631 \pm 0.252 \pm 0.058 \pm 0.850$
$[3, 4]$	$[-5.0, -2.5]$	$3.602 \pm 0.104 \pm 0.023 \pm 0.355$
$[4, 5]$	$[-5.0, -2.5]$	$1.601 \pm 0.055 \pm 0.013 \pm 0.175$
$[5, 6]$	$[-4.5, -2.5]$	$0.641 \pm 0.027 \pm 0.006 \pm 0.083$
$[6, 7]$	$[-4.5, -2.5]$	$0.340 \pm 0.018 \pm 0.004 \pm 0.047$
$[7, 8]$	$[-4.5, -2.5]$	$0.137 \pm 0.011 \pm 0.002 \pm 0.020$
$[8, 9]$	$[-4.0, -2.5]$	$0.069 \pm 0.007 \pm 0.002 \pm 0.010$
$[9, 10]$	$[-3.5, -2.5]$	$0.035 \pm 0.005 \pm 0.001 \pm 0.006$
$[10, 14]$	$[-3.5, -2.5]$	$0.009 \pm 0.001 \pm 0.000 \pm 0.001$

Table 7. Differential cross-section for prompt D_s^+ mesons as a function of p_{T} in the total forward and backward rapidity regions, respectively. The first uncertainty is statistical, the second is the component of the systematic uncertainty that is uncorrelated between bins and the third is the fully correlated component.

Forward

$p_{\mathrm{T}}\,[\mathrm{GeV}/c]$	y^*	$\frac{\mathrm{d}\sigma}{\mathrm{d}p_{\mathrm{T}}}\ [\mathrm{mb}/(\mathrm{GeV}/c)]$
$[0, 1]$	$[2.5, 4.0]$	$11.306 \pm 0.183 \pm 0.091 \pm 0.604$
$[1, 2]$	$[2.5, 4.0]$	$15.584 \pm 0.129 \pm 0.067 \pm 0.725$
$[2, 3]$	$[2.5, 4.0]$	$9.062 \pm 0.054 \pm 0.030 \pm 0.669$
$[3, 4]$	$[2.5, 4.0]$	$4.295 \pm 0.026 \pm 0.014 \pm 0.518$
$[4, 5]$	$[2.5, 4.0]$	$1.874 \pm 0.015 \pm 0.007 \pm 0.300$
$[5, 6]$	$[2.5, 4.0]$	$0.879 \pm 0.010 \pm 0.005 \pm 0.166$
$[6, 7]$	$[2.5, 4.0]$	$0.438 \pm 0.008 \pm 0.003 \pm 0.087$
$[7, 8]$	$[2.5, 4.0]$	$0.224 \pm 0.008 \pm 0.003 \pm 0.046$
$[8, 9]$	$[2.5, 3.5]$	$0.108 \pm 0.003 \pm 0.001 \pm 0.026$
$[9, 10]$	$[2.5, 3.5]$	$0.062 \pm 0.002 \pm 0.001 \pm 0.014$
$[10, 11]$	$[2.5, 3.5]$	$0.036 \pm 0.002 \pm 0.001 \pm 0.008$
$[11, 12]$	$[2.5, 3.5]$	$0.027 \pm 0.002 \pm 0.001 \pm 0.005$
$[12, 13]$	$[2.5, 3.0]$	$0.009 \pm 0.001 \pm 0.000 \pm 0.002$
$[13, 14]$	$[2.5, 3.0]$	$0.006 \pm 0.001 \pm 0.000 \pm 0.001$

Backward

$p_{\mathrm{T}}\,[\mathrm{GeV}/c]$	y^*	$\frac{\mathrm{d}\sigma}{\mathrm{d}p_{\mathrm{T}}}\ [\mathrm{mb}/(\mathrm{GeV}/c)]$
$[0, 1]$	$[-4.0, -3.0]$	$11.786 \pm 0.610 \pm 0.201 \pm 0.800$
$[1, 2]$	$[-4.0, -2.5]$	$20.026 \pm 0.362 \pm 0.146 \pm 1.242$
$[2, 3]$	$[-4.0, -2.5]$	$11.738 \pm 0.125 \pm 0.051 \pm 0.755$
$[3, 4]$	$[-4.0, -2.5]$	$5.320 \pm 0.053 \pm 0.021 \pm 0.505$
$[4, 5]$	$[-4.0, -2.5]$	$2.275 \pm 0.026 \pm 0.010 \pm 0.292$
$[5, 6]$	$[-4.0, -2.5]$	$1.026 \pm 0.015 \pm 0.005 \pm 0.157$
$[6, 7]$	$[-4.0, -2.5]$	$0.500 \pm 0.010 \pm 0.003 \pm 0.088$
$[7, 8]$	$[-4.0, -2.5]$	$0.244 \pm 0.006 \pm 0.002 \pm 0.047$
$[8, 9]$	$[-4.0, -2.5]$	$0.131 \pm 0.004 \pm 0.001 \pm 0.027$
$[9, 10]$	$[-4.0, -2.5]$	$0.073 \pm 0.003 \pm 0.001 \pm 0.016$
$[10, 11]$	$[-4.0, -2.5]$	$0.043 \pm 0.002 \pm 0.001 \pm 0.010$
$[11, 12]$	$[-4.0, -2.5]$	$0.026 \pm 0.002 \pm 0.001 \pm 0.006$
$[12, 13]$	$[-3.5, -2.5]$	$0.015 \pm 0.001 \pm 0.000 \pm 0.003$
$[13, 14]$	$[-3.5, -2.5]$	$0.009 \pm 0.001 \pm 0.000 \pm 0.002$

Table 8. Differential cross-section for prompt D^+ mesons as a function of p_{T} in the common forward and backward regions, respectively. The first uncertainty is statistical, the second is the component of the systematic uncertainty that is uncorrelated between bins and the third is the fully correlated component.

Forward

$p_{\mathrm{T}}\,[\,\mathrm{GeV}/c]$	y^*	$\frac{\mathrm{d}\sigma}{\mathrm{d}p_{\mathrm{T}}}\;[\,\mathrm{mb}/(\,\mathrm{GeV}/c)]$
$[0, 1]$	$[2.5, 4.0]$	$4.230 \pm 0.613 \pm 0.124 \pm 0.382$
$[1, 2]$	$[2.5, 4.0]$	$7.121 \pm 0.262 \pm 0.076 \pm 0.530$
$[2, 3]$	$[2.5, 4.0]$	$3.965 \pm 0.101 \pm 0.030 \pm 0.296$
$[3, 4]$	$[2.5, 4.0]$	$1.794 \pm 0.046 \pm 0.014 \pm 0.177$
$[4, 5]$	$[2.5, 4.0]$	$0.833 \pm 0.026 \pm 0.007 \pm 0.103$
$[5, 6]$	$[2.5, 4.0]$	$0.377 \pm 0.018 \pm 0.005 \pm 0.052$
$[6, 7]$	$[2.5, 4.0]$	$0.205 \pm 0.014 \pm 0.003 \pm 0.030$
$[7, 8]$	$[2.5, 3.5]$	$0.086 \pm 0.006 \pm 0.002 \pm 0.015$
$[8, 9]$	$[2.5, 3.5]$	$0.041 \pm 0.004 \pm 0.001 \pm 0.007$
$[9, 10]$	$[2.5, 3.5]$	$0.026 \pm 0.004 \pm 0.001 \pm 0.005$
$[10, 12]$	$[2.5, 3.0]$	$0.010 \pm 0.001 \pm 0.000 \pm 0.002$
$[12, 14]$	$[2.5, 3.0]$	$0.004 \pm 0.001 \pm 0.000 \pm 0.001$

Backward

$p_{\mathrm{T}}\,[\,\mathrm{GeV}/c]$	y^*	$\frac{\mathrm{d}\sigma}{\mathrm{d}p_{\mathrm{T}}}\;[\,\mathrm{mb}/(\,\mathrm{GeV}/c)]$
$[0, 1]$	$[-4.0, -3.0]$	$3.605 \pm 0.558 \pm 0.104 \pm 0.409$
$[1, 2]$	$[-4.0, -2.5]$	$10.097 \pm 0.506 \pm 0.125 \pm 1.186$
$[2, 3]$	$[-4.0, -2.5]$	$6.430 \pm 0.194 \pm 0.048 \pm 0.652$
$[3, 4]$	$[-4.0, -2.5]$	$2.945 \pm 0.087 \pm 0.020 \pm 0.294$
$[4, 5]$	$[-4.0, -2.5]$	$1.316 \pm 0.045 \pm 0.011 \pm 0.146$
$[5, 6]$	$[-4.0, -2.5]$	$0.558 \pm 0.025 \pm 0.005 \pm 0.072$
$[6, 7]$	$[-4.0, -2.5]$	$0.314 \pm 0.017 \pm 0.004 \pm 0.043$
$[7, 8]$	$[-4.0, -2.5]$	$0.118 \pm 0.010 \pm 0.002 \pm 0.017$
$[8, 9]$	$[-4.0, -2.5]$	$0.069 \pm 0.007 \pm 0.002 \pm 0.010$
$[9, 10]$	$[-3.5, -2.5]$	$0.035 \pm 0.005 \pm 0.001 \pm 0.006$
$[10, 14]$	$[-3.5, -2.5]$	$0.009 \pm 0.001 \pm 0.000 \pm 0.001$

Table 9. Differential cross-section for prompt D_s^+ mesons as a function of p_{T} in the common forward and backward regions, respectively. The first uncertainty is statistical, the second is the component of the systematic uncertainty that is uncorrelated between bins and the third is the fully correlated component.

Forward	
y^*	$\frac{\mathrm{d}\sigma}{\mathrm{d}y^*}$ [mb]
$[1.5, 2.0]$	$35.87 \pm 1.24 \pm 2.08$
$[2.0, 2.5]$	$36.41 \pm 0.27 \pm 2.95$
$[2.5, 3.0]$	$34.84 \pm 0.21 \pm 2.73$
$[3.0, 3.5]$	$29.70 \pm 0.23 \pm 1.86$
$[3.5, 4.0]$	$23.28 \pm 0.34 \pm 1.21$
Backward	
y^*	$\frac{\mathrm{d}\sigma}{\mathrm{d}y^*}$ [mb]
$[-3.0, -2.5]$	$35.81 \pm 1.32 \pm 2.49$
$[-3.5, -3.0]$	$36.28 \pm 0.44 \pm 2.49$
$[-4.0, -3.5]$	$34.33 \pm 0.40 \pm 2.14$
$[-4.5, -4.0]$	$27.86 \pm 0.53 \pm 1.65$
$[-5.0, -4.5]$	$21.14 \pm 0.91 \pm 1.67$

Table 10. Differential cross-section for prompt D^+ mesons as a function of $|y^*|$ integrated over $1 < p_{\mathrm{T}} < 14\,\mathrm{GeV}/c$ for the forward and backward regions, respectively. The first uncertainty is statistical, the second is systematic.

Forward	
y^*	$\frac{\mathrm{d}\sigma}{\mathrm{d}y^*}$ [mb]
$[1.5, 2.0]$	$13.37 \pm 0.58 \pm 1.42$
$[2.0, 2.5]$	$12.93 \pm 0.26 \pm 1.26$
$[2.5, 3.0]$	$13.04 \pm 0.25 \pm 1.10$
$[3.0, 3.5]$	$9.38 \pm 0.26 \pm 0.73$
$[3.5, 4.0]$	$6.52 \pm 0.45 \pm 0.51$
Backward	
y^*	$\frac{\mathrm{d}\sigma}{\mathrm{d}y^*}$ [mb]
$[-3.0, -2.5]$	$15.71 \pm 0.89 \pm 2.07$
$[-3.5, -3.0]$	$14.25 \pm 0.45 \pm 1.12$
$[-4.0, -3.5]$	$13.88 \pm 0.47 \pm 1.20$
$[-4.5, -4.0]$	$9.88 \pm 0.58 \pm 1.14$
$[-5.0, -4.5]$	$3.76 \pm 0.92 \pm 0.94$

Table 11. Differential cross-section for prompt D_s^+ mesons as a function of $|y^*|$ integrated over $1 < p_{\mathrm{T}} < 14\,\mathrm{GeV}/c$ for the forward and backward regions, respectively. The first uncertainty is statistical, the second is systematic.

B Nuclear modification factor $R_{p\mathrm{Pb}}$

Tables 12–13 give the numerical results for the nuclear modification factor as a function of p_{T}. Tables 14–15 give the numerical results for the nuclear modification factor as a function of y^*.

p_{T} [GeV/c]	Forward	Backward
$[0, 1]$	$0.585^{+0.029+0.052}_{-0.029-0.048}$	$0.610^{+0.042+0.070}_{-0.042-0.066}$
$[1, 2]$	$0.606^{+0.006+0.033}_{-0.006-0.032}$	$0.779^{+0.015+0.069}_{-0.015-0.067}$
$[2, 3]$	$0.634^{+0.005+0.028}_{-0.005-0.028}$	$0.822^{+0.009+0.060}_{-0.009-0.061}$
$[3, 4]$	$0.678^{+0.005+0.024}_{-0.005-0.029}$	$0.839^{+0.009+0.053}_{-0.009-0.057}$
$[4, 5]$	$0.684^{+0.007+0.025}_{-0.007-0.027}$	$0.831^{+0.011+0.051}_{-0.011-0.053}$
$[5, 6]$	$0.698^{+0.010+0.026}_{-0.010-0.028}$	$0.814^{+0.013+0.048}_{-0.013-0.050}$
$[6, 7]$	$0.723^{+0.015+0.031}_{-0.015-0.032}$	$0.825^{+0.018+0.050}_{-0.018-0.050}$
$[7, 8]$	$0.715^{+0.028+0.036}_{-0.028-0.037}$	$0.778^{+0.023+0.048}_{-0.023-0.048}$
$[8, 9]$	$0.806^{+0.030+0.052}_{-0.030-0.050}$	$0.975^{+0.043+0.066}_{-0.043-0.065}$
$[9, 10]$	$0.847^{+0.045+0.065}_{-0.045-0.060}$	$1.002^{+0.056+0.077}_{-0.056-0.073}$

Table 12. Nuclear modification factor $R_{p\mathrm{Pb}}$ for prompt D^+ meson production in different p_{T} intervals, for the forward and backward rapidity regions. The first uncertainty is statistical, the second is systematic.

p_{T} [GeV/c]	Forward	Backward
$[1, 2]$	$0.665^{+0.036+0.047}_{-0.036-0.044}$	$0.944^{+0.060+0.121}_{-0.060-0.119}$
$[2, 3]$	$0.592^{+0.019+0.028}_{-0.019-0.027}$	$0.960^{+0.034+0.097}_{-0.034-0.096}$
$[3, 4]$	$0.587^{+0.019+0.026}_{-0.019-0.024}$	$0.964^{+0.034+0.077}_{-0.034-0.075}$
$[4, 5]$	$0.614^{+0.022+0.027}_{-0.022-0.025}$	$0.971^{+0.038+0.068}_{-0.038-0.066}$
$[5, 6]$	$0.621^{+0.036+0.030}_{-0.036-0.025}$	$0.920^{+0.051+0.064}_{-0.051-0.059}$
$[6, 7]$	$0.720^{+0.057+0.043}_{-0.057-0.034}$	$1.101^{+0.078+0.080}_{-0.078-0.069}$
$[7, 8]$	$0.748^{+0.076+0.062}_{-0.076-0.039}$	$1.030^{+0.116+0.083}_{-0.116-0.066}$
$[8, 9]$	$0.687^{+0.092+0.058}_{-0.092-0.039}$	$0.981^{+0.145+0.093}_{-0.145-0.070}$
$[9, 10]$	$0.709^{+0.123+0.070}_{-0.123-0.048}$	$0.931^{+0.170+0.099}_{-0.170-0.075}$

Table 13. Nuclear modification factor $R_{p\mathrm{Pb}}$ for prompt D_s^+ meson production in different p_{T} intervals, for the forward and backward rapidity regions. The first uncertainty is statistical, the second is systematic.

y^*	$R_{p\mathrm{Pb}}$
$[-4.5, -4.0]$	$1.018^{+\,0.031}_{-\,0.031}{}^{+\,0.074}_{-\,0.071}$
$[-4.0, -3.5]$	$0.875^{+\,0.022}_{-\,0.022}{}^{+\,0.062}_{-\,0.059}$
$[-3.5, -3.0]$	$0.765^{+\,0.015}_{-\,0.015}{}^{+\,0.066}_{-\,0.062}$
$[-3.0, -2.5]$	$0.649^{+\,0.029}_{-\,0.029}{}^{+\,0.065}_{-\,0.065}$
$[2.0, 2.5]$	$0.710^{+\,0.013}_{-\,0.013}{}^{+\,0.062}_{-\,0.056}$
$[2.5, 3.0]$	$0.632^{+\,0.017}_{-\,0.017}{}^{+\,0.038}_{-\,0.039}$
$[3.0, 3.5]$	$0.626^{+\,0.011}_{-\,0.011}{}^{+\,0.032}_{-\,0.027}$
$[3.5, 4.0]$	$0.594^{+\,0.016}_{-\,0.016}{}^{+\,0.036}_{-\,0.033}$

Table 14. Nuclear modification factor $R_{p\mathrm{Pb}}$ for prompt D^+ meson production in different y^* intervals, integrated up to $p_{\mathrm{T}} = 10\,\mathrm{GeV}/c$. The first uncertainty is statistical, the second is systematic.

y^*	$R_{p\mathrm{Pb}}$
$[-4.5, -4.0]$	$1.264^{+\,0.191}_{-\,0.191}{}^{+\,0.134}_{-\,0.111}$
$[-4.0, -3.5]$	$1.275^{+\,0.073}_{-\,0.073}{}^{+\,0.104}_{-\,0.093}$
$[-3.5, -3.0]$	$0.895^{+\,0.039}_{-\,0.039}{}^{+\,0.089}_{-\,0.084}$
$[-3.0, -2.5]$	$0.821^{+\,0.052}_{-\,0.052}{}^{+\,0.123}_{-\,0.124}$
$[2.0, 2.5]$	$0.760^{+\,0.048}_{-\,0.048}{}^{+\,0.093}_{-\,0.073}$
$[2.5, 3.0]$	$0.680^{+\,0.024}_{-\,0.024}{}^{+\,0.036}_{-\,0.038}$
$[3.0, 3.5]$	$0.591^{+\,0.024}_{-\,0.024}{}^{+\,0.036}_{-\,0.030}$
$[3.5, 4.0]$	$0.601^{+\,0.050}_{-\,0.050}{}^{+\,0.044}_{-\,0.038}$

Table 15. Nuclear modification factor $R_{p\mathrm{Pb}}$ for prompt D_s^+ meson production in different y^* intervals, integrated up to $p_{\mathrm{T}} = 10\,\mathrm{GeV}/c$. The first uncertainty is statistical, the second is systematic.

C Forward-backward production ratios of D^+ and D_s^+

Tables 16–17 give the numerical results for the forward-backward production ratios.

p_{T} [GeV/c]	R_{FB}
$[0, 1]$	$0.959 \pm 0.052 \pm 0.092$
$[1, 2]$	$0.778 \pm 0.015 \pm 0.062$
$[2, 3]$	$0.772 \pm 0.009 \pm 0.048$
$[3, 4]$	$0.807 \pm 0.009 \pm 0.042$
$[4, 5]$	$0.823 \pm 0.012 \pm 0.040$
$[5, 6]$	$0.857 \pm 0.016 \pm 0.039$
$[6, 7]$	$0.876 \pm 0.023 \pm 0.042$
$[7, 8]$	$0.919 \pm 0.041 \pm 0.051$
$[8, 9]$	$1.046 \pm 0.052 \pm 0.057$
$[9, 10]$	$1.061 \pm 0.071 \pm 0.068$
$[10, 11]$	$0.987 \pm 0.088 \pm 0.079$
$[11, 12]$	$1.241 \pm 0.152 \pm 0.167$
$[12, 13]$	$0.877 \pm 0.135 \pm 0.089$
$[13, 14]$	$0.902 \pm 0.189 \pm 0.107$
$\lvert y^* \rvert$	R_{FB}
$[2.5, 3.0]$	$0.973 \pm 0.036 \pm 0.089$
$[3.0, 3.5]$	$0.819 \pm 0.012 \pm 0.058$
$[3.5, 4.0]$	$0.680 \pm 0.013 \pm 0.043$

Table 16. Forward-backward production ratios of D^+ mesons as a function of p_{T}, integrated over the common rapidity range $2.5 < |y^*| < 4.0$; and as a function of y^*, integrated over $0 < p_{\mathrm{T}} < 14\,\mathrm{GeV}/c$. The first uncertainty is statistical, the second is systematic.

p_{T} [GeV/c]	R_{FB}
$[0, 1]$	$0.775 \pm 0.208 \pm 0.104$
$[1, 2]$	$0.705 \pm 0.044 \pm 0.086$
$[2, 3]$	$0.617 \pm 0.024 \pm 0.056$
$[3, 4]$	$0.609 \pm 0.024 \pm 0.042$
$[4, 5]$	$0.633 \pm 0.029 \pm 0.036$
$[5, 6]$	$0.675 \pm 0.045 \pm 0.036$
$[6, 7]$	$0.654 \pm 0.057 \pm 0.036$
$[7, 8]$	$0.929 \pm 0.119 \pm 0.047$
$[8, 9]$	$0.701 \pm 0.111 \pm 0.041$
$[9, 10]$	$0.762 \pm 0.155 \pm 0.054$
$[10, 14]$	$1.337 \pm 0.323 \pm 0.089$
$\lvert y^* \rvert$	R_{FB}
$[2.5, 3.0]$	$0.830 \pm 0.054 \pm 0.119$
$[3.0, 3.5]$	$0.715 \pm 0.049 \pm 0.071$
$[3.5, 4.0]$	$0.502 \pm 0.071 \pm 0.041$

Table 17. Forward-backward production ratios of D_s^+ mesons as a function of p_{T}, integrated over the common rapidity range $2.5 < |y^*| < 4.0$; and as a function of y^*, integrated over $0 < p_{\mathrm{T}} < 14\,\mathrm{GeV}/c$. The first uncertainty is statistical, the second is systematic.

D Production ratios between D^+, D_s^+ and D^0

Tables 18–20 give the numerical results for the cross-section ratios between mesons as a function of p_{T}. Tables 21–23 give the numerical results for the cross-section ratios between mesons as a function of y^*.

p_{T} [GeV/c]	Forward	Backward
$[0, 1]$	$0.337 \pm 0.011 \pm 0.031$	$0.302 \pm 0.012 \pm 0.036$
$[1, 2]$	$0.334 \pm 0.004 \pm 0.023$	$0.302 \pm 0.005 \pm 0.029$
$[2, 3]$	$0.351 \pm 0.002 \pm 0.017$	$0.311 \pm 0.003 \pm 0.024$
$[3, 4]$	$0.373 \pm 0.002 \pm 0.016$	$0.325 \pm 0.004 \pm 0.024$
$[4, 5]$	$0.378 \pm 0.003 \pm 0.017$	$0.330 \pm 0.005 \pm 0.024$
$[5, 6]$	$0.391 \pm 0.005 \pm 0.026$	$0.339 \pm 0.009 \pm 0.030$
$[6, 7]$	$0.406 \pm 0.009 \pm 0.035$	$0.360 \pm 0.009 \pm 0.027$
$[7, 8]$	$0.402 \pm 0.010 \pm 0.028$	$0.332 \pm 0.012 \pm 0.035$
$[8, 9]$	$0.418 \pm 0.010 \pm 0.039$	$0.350 \pm 0.020 \pm 0.060$
$[9, 10]$	$0.418 \pm 0.015 \pm 0.046$	$0.339 \pm 0.023 \pm 0.038$

Table 18. Measured of R_{D^+/D^0} as a function of p_{T} in LHCb pPb collisions at 5.02 TeV in the forward and backward regions, integrated over $2.5 < |y^*| < 4.0$. The first uncertainty is statistical, the second is systematic.

p_{T} [GeV/c]	Forward	Backward
$[0, 1]$	$0.139 \pm 0.015 \pm 0.014$	$0.162 \pm 0.023 \pm 0.025$
$[1, 2]$	$0.146 \pm 0.005 \pm 0.012$	$0.140 \pm 0.007 \pm 0.018$
$[2, 3]$	$0.159 \pm 0.003 \pm 0.010$	$0.165 \pm 0.005 \pm 0.016$
$[3, 4]$	$0.167 \pm 0.003 \pm 0.008$	$0.170 \pm 0.005 \pm 0.014$
$[4, 5]$	$0.179 \pm 0.004 \pm 0.009$	$0.186 \pm 0.007 \pm 0.015$
$[5, 6]$	$0.188 \pm 0.006 \pm 0.013$	$0.193 \pm 0.009 \pm 0.013$
$[6, 7]$	$0.193 \pm 0.008 \pm 0.017$	$0.217 \pm 0.012 \pm 0.017$
$[7, 8]$	$0.181 \pm 0.008 \pm 0.013$	$0.169 \pm 0.015 \pm 0.018$
$[8, 9]$	$0.175 \pm 0.011 \pm 0.017$	$0.193 \pm 0.022 \pm 0.019$
$[9, 10]$	$0.190 \pm 0.015 \pm 0.022$	$0.198 \pm 0.031 \pm 0.019$

Table 19. Measured of $R_{D_s^+/D^0}$ ratio as a function of p_{T} in LHCb pPb collisions at 5.02 TeV in the forward and backward regions, integrated over $2.5 < |y^*| < 4.0$. The first uncertainty is statistical, the second is systematic.

$p_{\mathrm{T}}\,[\mathrm{GeV}/c]$	Forward	Backward
$[0, 1]$	$0.393 \pm 0.046 \pm 0.041$	$0.532 \pm 0.082 \pm 0.081$
$[1, 2]$	$0.438 \pm 0.015 \pm 0.036$	$0.462 \pm 0.026 \pm 0.057$
$[2, 3]$	$0.451 \pm 0.009 \pm 0.025$	$0.531 \pm 0.016 \pm 0.050$
$[3, 4]$	$0.449 \pm 0.009 \pm 0.018$	$0.524 \pm 0.016 \pm 0.038$
$[4, 5]$	$0.474 \pm 0.010 \pm 0.014$	$0.565 \pm 0.020 \pm 0.033$
$[5, 6]$	$0.480 \pm 0.014 \pm 0.013$	$0.547 \pm 0.025 \pm 0.027$
$[6, 7]$	$0.475 \pm 0.019 \pm 0.015$	$0.603 \pm 0.034 \pm 0.029$
$[7, 8]$	$0.451 \pm 0.022 \pm 0.012$	$0.509 \pm 0.044 \pm 0.024$
$[8, 9]$	$0.419 \pm 0.025 \pm 0.014$	$0.523 \pm 0.056 \pm 0.028$
$[9, 10]$	$0.454 \pm 0.036 \pm 0.018$	$0.598 \pm 0.098 \pm 0.037$
$[10, 12]$	$0.486 \pm 0.040 \pm 0.018$	—
$[12, 14]$	$0.469 \pm 0.065 \pm 0.028$	—
$[10, 14]$	—	$0.426 \pm 0.070 \pm 0.026$

Table 20. Measured of $R_{D_s^+/D^+}$ ratio as a function of p_{T} in LHCb pPb collisions at 5.02 TeV in the forward and backward regions, integrated over $2.5 < |y^*| < 4.0$. The first uncertainty is statistical, the second is systematic.

$\lvert y^*\rvert$	Forward	Backward
$[1.5, 2.0]$	$0.311 \pm 0.011 \pm 0.030$	—
$[2.0, 2.5]$	$0.340 \pm 0.003 \pm 0.024$	—
$[2.5, 3.0]$	$0.371 \pm 0.003 \pm 0.017$	$0.283 \pm 0.011 \pm 0.041$
$[3.0, 3.5]$	$0.368 \pm 0.003 \pm 0.014$	$0.301 \pm 0.004 \pm 0.027$
$[3.5, 4.0]$	$0.362 \pm 0.006 \pm 0.028$	$0.328 \pm 0.004 \pm 0.022$
$[4.0, 4.5]$	—	$0.317 \pm 0.007 \pm 0.023$
$[4.5, 5.0]$	—	$0.325 \pm 0.016 \pm 0.039$

Table 21. Measured of R_{D^+/D^0} as a function of $|y^*|$ in LHCb pPb collisions at 5.02 TeV in the forward and backward regions, integrated over $0 < p_{\mathrm{T}} < 10\,\mathrm{GeV}/c$. The first uncertainty is statistical, the second is systematic.

$\lvert y^*\rvert$	Forward	Backward
$[1.5, 2.0]$	$0.147 \pm 0.006 \pm 0.016$	—
$[2.0, 2.5]$	$0.151 \pm 0.005 \pm 0.012$	—
$[2.5, 3.0]$	$0.169 \pm 0.005 \pm 0.008$	$0.159 \pm 0.009 \pm 0.027$
$[3.0, 3.5]$	$0.159 \pm 0.007 \pm 0.008$	$0.149 \pm 0.008 \pm 0.016$
$[3.5, 4.0]$	$0.135 \pm 0.018 \pm 0.012$	$0.166 \pm 0.009 \pm 0.013$
$[4.0, 4.5]$	—	$0.183 \pm 0.019 \pm 0.024$
$[4.5, 5.0]$	—	$0.086 \pm 0.021 \pm 0.013$

Table 22. Measured of $R_{D_s^+/D^0}$ as a function of $\lvert y^*\rvert$ in LHCb pPb collisions at 5.02 TeV in the forward and backward regions, integrated over $0 < p_{\mathrm{T}} < 10\,\mathrm{GeV}/c$. The first uncertainty is statistical, the second is systematic.

$\lvert y^*\rvert$	Forward	Backward
$[1.5, 2.0]$	$0.460 \pm 0.028 \pm 0.045$	—
$[2.0, 2.5]$	$0.444 \pm 0.014 \pm 0.039$	—
$[2.5, 3.0]$	$0.457 \pm 0.013 \pm 0.024$	$0.535 \pm 0.039 \pm 0.084$
$[3.0, 3.5]$	$0.433 \pm 0.020 \pm 0.018$	$0.496 \pm 0.026 \pm 0.053$
$[3.5, 4.0]$	$0.373 \pm 0.049 \pm 0.026$	$0.506 \pm 0.027 \pm 0.034$
$[4.0, 4.5]$	—	$0.578 \pm 0.061 \pm 0.069$
$[4.5, 5.0]$	—	$0.290 \pm 0.074 \pm 0.037$

Table 23. Measured $R_{D_s^+/D^+}$ as a function of $\lvert y^*\rvert$ in LHCb pPb collisions at 5.02 TeV in the forward and backward regions, integrated over $0 < p_{\mathrm{T}} < 10\,\mathrm{GeV}/c$. The first uncertainty is statistical, the second is systematic.

References

[1] E.V. Shuryak, *Quantum chromodynamics and the theory of superdense matter*, Phys. Rept. **61** (1980) 71 [INSPIRE].

[2] STAR collaboration, *Observation of D^0 meson nuclear modifications in Au+Au collisions at $\sqrt{s_{\rm NN}} = 200$ GeV*, Phys. Rev. Lett. **113** (2014) 142301 [*Erratum ibid.* **121** (2018) 229901] [`arXiv:1404.6185`] [INSPIRE].

[3] STAR collaboration, *Centrality and transverse momentum dependence of D^0-meson production at mid-rapidity in Au+Au collisions at $\sqrt{s_{\rm NN}} = 200$ GeV*, Phys. Rev. C **99** (2019) 034908 [`arXiv:1812.10224`] [INSPIRE].

[4] ALICE collaboration, *Transverse momentum dependence of D-meson production in Pb-Pb collisions at $\sqrt{s_{\rm NN}} = 2.76$ TeV*, JHEP **03** (2016) 081 [`arXiv:1509.06888`] [INSPIRE].

[5] ALICE collaboration, *Measurement of D_s^+ production and nuclear modification factor in Pb-Pb collisions at $\sqrt{s_{\rm NN}} = 2.76$ TeV*, JHEP **03** (2016) 082 [`arXiv:1509.07287`] [INSPIRE].

[6] ALICE collaboration, *Prompt D^0, D^+, and D^{*+} production in Pb-Pb collisions at $\sqrt{s_{\rm NN}} = 5.02$ TeV*, JHEP **01** (2022) 174 [`arXiv:2110.09420`] [INSPIRE].

[7] S. Wicks, W. Horowitz, M. Djordjevic and M. Gyulassy, *Elastic, inelastic, and path length fluctuations in jet tomography*, Nucl. Phys. A **784** (2007) 426 [`nucl-th/0512076`] [INSPIRE].

[8] J. Uphoff, O. Fochler, Z. Xu and C. Greiner, *Open heavy flavor in Pb+Pb collisions at $\sqrt{s} = 2.76$ TeV within a transport model*, Phys. Lett. B **717** (2012) 430 [`arXiv:1205.4945`] [INSPIRE].

[9] M. He, R.J. Fries and R. Rapp, *Heavy flavor at the Large Hadron Collider in a strong coupling approach*, Phys. Lett. B **735** (2014) 445 [`arXiv:1401.3817`] [INSPIRE].

[10] W.A. Horowitz, *Testing pQCD and AdS/CFT energy loss at RHIC and LHC*, AIP Conf. Proc. **1441** (2012) 889 [`arXiv:1108.5876`] [INSPIRE].

[11] STAR collaboration, *Observation of $D_s^\pm/D^0$ enhancement in Au+Au collisions at $\sqrt{s_{\rm NN}} = 200$ GeV*, Phys. Rev. Lett. **127** (2021) 092301 [`arXiv:2101.11793`] [INSPIRE].

[12] ALICE collaboration, *Measurement of prompt D_s^+-meson production and azimuthal anisotropy in Pb-Pb collisions at $\sqrt{s_{\rm NN}} = 5.02$ TeV*, Phys. Lett. B **827** (2022) 136986 [`arXiv:2110.10006`] [INSPIRE].

[13] ALICE collaboration, *Measurement of D^0, D^+, D^{*+} and D_s^+ production in Pb-Pb collisions at $\sqrt{s_{\rm NN}} = 5.02$ TeV*, JHEP **10** (2018) 174 [`arXiv:1804.09083`] [INSPIRE].

[14] ALICE collaboration, *Measurement of beauty and charm production in pp collisions at $\sqrt{s} = 5.02$ TeV via non-prompt and prompt D mesons*, JHEP **05** (2021) 220 [`arXiv:2102.13601`] [INSPIRE].

[15] ALICE collaboration, *Measurement of D^0, D^+, D^{*+} and D_s^+ production in pp collisions at $\sqrt{s} = 5.02$ TeV with ALICE*, Eur. Phys. J. C **79** (2019) 388 [`arXiv:1901.07979`] [INSPIRE].

[16] T. Sjöstrand, S. Mrenna and P.Z. Skands, *PYTHIA 6.4 physics and manual*, JHEP **05** (2006) 026 [`hep-ph/0603175`] [INSPIRE].

[17] C. Bierlich and J.R. Christiansen, *Effects of color reconnection on hadron flavor observables*, *Phys. Rev. D* **92** (2015) 094010 [`arXiv:1507.02091`] [INSPIRE].

[18] V. Greco, C.M. Ko and P. Levai, *Parton coalescence and anti-proton/pion anomaly at RHIC*, *Phys. Rev. Lett.* **90** (2003) 202302 [`nucl-th/0301093`] [INSPIRE].

[19] R.J. Fries, B. Muller, C. Nonaka and S.A. Bass, *Hadronization in heavy ion collisions: recombination and fragmentation of partons*, *Phys. Rev. Lett.* **90** (2003) 202303 [`nucl-th/0301087`] [INSPIRE].

[20] V. Greco, C.M. Ko and P. Levai, *Parton coalescence at RHIC*, *Phys. Rev. C* **68** (2003) 034904 [`nucl-th/0305024`] [INSPIRE].

[21] L. Ravagli and R. Rapp, *Quark coalescence based on a transport equation*, *Phys. Lett. B* **655** (2007) 126 [`arXiv:0705.0021`] [INSPIRE].

[22] D. Kharzeev and K. Tuchin, *Signatures of the color glass condensate in J/ψ production off nuclear targets*, *Nucl. Phys. A* **770** (2006) 40 [`hep-ph/0510358`] [INSPIRE].

[23] H. Fujii, F. Gelis and R. Venugopalan, *Quark pair production in high energy pA collisions: general features*, *Nucl. Phys. A* **780** (2006) 146 [`hep-ph/0603099`] [INSPIRE].

[24] N. Armesto, *Nuclear shadowing*, *J. Phys. G* **32** (2006) R367 [`hep-ph/0604108`] [INSPIRE].

[25] H. Fujii and K. Watanabe, *Heavy quark pair production in high energy pA collisions: open heavy flavors*, *Nucl. Phys. A* **920** (2013) 78 [`arXiv:1308.1258`] [INSPIRE].

[26] P. Tribedy and R. Venugopalan, *QCD saturation at the LHC: comparisons of models to p+p and A+A data and predictions for p+Pb collisions*, *Phys. Lett. B* **710** (2012) 125 [*Erratum ibid.* **718** (2013) 1154] [`arXiv:1112.2445`] [INSPIRE].

[27] J.L. Albacete, A. Dumitru, H. Fujii and Y. Nara, *CGC predictions for p+Pb collisions at the LHC*, *Nucl. Phys. A* **897** (2013) 1 [`arXiv:1209.2001`] [INSPIRE].

[28] A.H. Rezaeian, *CGC predictions for p+A collisions at the LHC and signature of QCD saturation*, *Phys. Lett. B* **718** (2013) 1058 [`arXiv:1210.2385`] [INSPIRE].

[29] PHENIX collaboration, *Cold-nuclear-matter effects on heavy-quark production in d+Au collisions at $\sqrt{s_{\rm NN}} = 200$ GeV*, *Phys. Rev. Lett.* **109** (2012) 242301 [`arXiv:1208.1293`] [INSPIRE].

[30] PHENIX collaboration, *Cold-nuclear-matter effects on heavy-quark production at forward and backward rapidity in d+Au collisions at $\sqrt{s_{\rm NN}} = 200$ GeV*, *Phys. Rev. Lett.* **112** (2014) 252301 [`arXiv:1310.1005`] [INSPIRE].

[31] ALICE collaboration, *Measurement of electrons from heavy-flavour hadron decays in p-Pb collisions at $\sqrt{s_{\rm NN}} = 5.02$ TeV*, *Phys. Lett. B* **754** (2016) 81 [`arXiv:1509.07491`] [INSPIRE].

[32] ALICE collaboration, *Measurement of electrons from beauty-hadron decays in p-Pb collisions at $\sqrt{s_{\rm NN}} = 5.02$ TeV and Pb-Pb collisions at $\sqrt{s_{\rm NN}} = 2.76$ TeV*, *JHEP* **07** (2017) 052 [`arXiv:1609.03898`] [INSPIRE].

[33] ALICE collaboration, *Production of muons from heavy-flavour hadron decays in p-Pb collisions at $\sqrt{s_{\rm NN}} = 5.02$ TeV*, *Phys. Lett. B* **770** (2017) 459 [`arXiv:1702.01479`] [INSPIRE].

[34] LHCb collaboration, *Study of J/ψ production and cold nuclear matter effects in pPb collisions at $\sqrt{s_{\rm NN}} = 5$ TeV*, *JHEP* **02** (2014) 072 [`arXiv:1308.6729`] [INSPIRE].

[35] LHCb collaboration, *Study of $\psi(2S)$ production and cold nuclear matter effects in pPb collisions at $\sqrt{s_{\rm NN}} = 5$ TeV*, *JHEP* **03** (2016) 133 [`arXiv:1601.07878`] [INSPIRE].

[36] LHCb collaboration, *Study of prompt D^0 meson production in pPb collisions at $\sqrt{s_{\rm NN}} = 5$ TeV*, *JHEP* **10** (2017) 090 [`arXiv:1707.02750`] [INSPIRE].

[37] LHCb collaboration, *Prompt Λ_c^+ production in pPb collisions at $\sqrt{s_{\rm NN}} = 5.02$ TeV*, *JHEP* **02** (2019) 102 [`arXiv:1809.01404`] [INSPIRE].

[38] ALICE collaboration, *Measurement of prompt D^0, D^+, D^{*+}, and $D_{\rm S}^+$ production in p-Pb collisions at $\sqrt{s_{\rm NN}} = 5.02$ TeV*, *JHEP* **12** (2019) 092 [`arXiv:1906.03425`] [INSPIRE].

[39] ALICE collaboration, *J/ψ production as a function of charged-particle pseudorapidity density in p-Pb collisions at $\sqrt{s_{\rm NN}} = 5.02$ TeV*, *Phys. Lett. B* **776** (2018) 91 [`arXiv:1704.00274`] [INSPIRE].

[40] ALICE collaboration, *D-meson production in p-Pb collisions at $\sqrt{s_{\rm NN}} = 5.02$ TeV and in pp collisions at $\sqrt{s} = 7$ TeV*, *Phys. Rev. C* **94** (2016) 054908 [`arXiv:1605.07569`] [INSPIRE].

[41] ALICE collaboration, *Centrality dependence of $\psi(2S)$ suppression in p-Pb collisions at $\sqrt{s_{\rm NN}} = 5.02$ TeV*, *JHEP* **06** (2016) 050 [`arXiv:1603.02816`] [INSPIRE].

[42] ALICE collaboration, *Measurement of D-meson production versus multiplicity in p-Pb collisions at $\sqrt{s_{\rm NN}} = 5.02$ TeV*, *JHEP* **08** (2016) 078 [`arXiv:1602.07240`] [INSPIRE].

[43] ALICE collaboration, *Centrality dependence of inclusive J/ψ production in p-Pb collisions at $\sqrt{s_{\rm NN}} = 5.02$ TeV*, *JHEP* **11** (2015) 127 [`arXiv:1506.08808`] [INSPIRE].

[44] ALICE collaboration, *Measurement of prompt D-meson production in p-Pb collisions at $\sqrt{s_{\rm NN}} = 5.02$ TeV*, *Phys. Rev. Lett.* **113** (2014) 232301 [`arXiv:1405.3452`] [INSPIRE].

[45] ALICE collaboration, *J/ψ production and nuclear effects in p-Pb collisions at $\sqrt{s_{\rm NN}} = 5.02$ TeV*, *JHEP* **02** (2014) 073 [`arXiv:1308.6726`] [INSPIRE].

[46] CMS collaboration, *Measurement of prompt and nonprompt J/ψ production in pp and pPb collisions at $\sqrt{s_{\rm NN}} = 5.02$ TeV*, *Eur. Phys. J. C* **77** (2017) 269 [`arXiv:1702.01462`] [INSPIRE].

[47] CMS collaboration, *Measurements of the charm jet cross section and nuclear modification factor in pPb collisions at $\sqrt{s_{\rm NN}} = 5.02$ TeV*, *Phys. Lett. B* **772** (2017) 306 [`arXiv:1612.08972`] [INSPIRE].

[48] LHCb collaboration, *Measurement of the prompt D^0 nuclear modification factor in p-Pb collisions at $\sqrt{s_{\rm NN}} = 8.16$ TeV*, *Phys. Rev. Lett.* **131** (2023) 102301 [`arXiv:2205.03936`] [INSPIRE].

[49] LHCb collaboration, *Observation of strangeness enhancement with charmed mesons in high-multiplicity pPb collisions at $\sqrt{s_{\rm NN}} = 8.16$ TeV*, `arXiv:2311.08490` [INSPIRE].

[50] K.J. Eskola, I. Helenius, P. Paakkinen and H. Paukkunen, *A QCD analysis of LHCb D-meson data in p+Pb collisions*, *JHEP* **05** (2020) 037 [`arXiv:1906.02512`] [INSPIRE].

[51] R. Abdul Khalek et al., *nNNPDF3.0: evidence for a modified partonic structure in heavy nuclei*, *Eur. Phys. J. C* **82** (2022) 507 [`arXiv:2201.12363`] [INSPIRE].

[52] LHCb collaboration, *The LHCb detector at the LHC*, 2008 *JINST* **3** S08005 [INSPIRE].

[53] LHCb collaboration, *Measurements of prompt charm production cross-sections in pp collisions at $\sqrt{s} = 5$ TeV*, *JHEP* **06** (2017) 147 [`arXiv:1610.02230`] [INSPIRE].

[54] LHCb collaboration, *LHCb detector performance*, *Int. J. Mod. Phys. A* **30** (2015) 1530022 [`arXiv:1412.6352`] [INSPIRE].

[55] C. Abellán Beteta et al., *Calibration and performance of the LHCb calorimeters in run 1 and 2 at the LHC*, `arXiv:2008.11556` [INSPIRE].

[56] R. Aaij et al., *The LHCb trigger and its performance in* 2011, 2013 *JINST* **8** P04022 [`arXiv:1211.3055`] [INSPIRE].

[57] T. Sjöstrand, S. Mrenna and P.Z. Skands, *A brief introduction to PYTHIA* 8.1, *Comput. Phys. Commun.* **178** (2008) 852 [`arXiv:0710.3820`] [INSPIRE].

[58] T. Pierog et al., *EPOS LHC: test of collective hadronization with data measured at the CERN Large Hadron Collider*, *Phys. Rev. C* **92** (2015) 034906 [`arXiv:1306.0121`] [INSPIRE].

[59] LHCb collaboration, *Handling of the generation of primary events in Gauss, the LHCb simulation framework*, *J. Phys. Conf. Ser.* **331** (2011) 032047 [INSPIRE].

[60] D.J. Lange, *The EvtGen particle decay simulation package*, *Nucl. Instrum. Meth. A* **462** (2001) 152 [INSPIRE].

[61] P. Golonka and Z. Was, *PHOTOS Monte Carlo: a precision tool for QED corrections in Z and W decays*, *Eur. Phys. J. C* **45** (2006) 97 [`hep-ph/0506026`] [INSPIRE].

[62] J. Allison et al., *GEANT4 developments and applications*, *IEEE Trans. Nucl. Sci.* **53** (2006) 270 [INSPIRE].

[63] GEANT4 collaboration, *GEANT4 — a simulation toolkit*, *Nucl. Instrum. Meth. A* **506** (2003) 250 [INSPIRE].

[64] LHCb collaboration, *The LHCb simulation application, Gauss: design, evolution and experience*, *J. Phys. Conf. Ser.* **331** (2011) 032023 [INSPIRE].

[65] PARTICLE DATA GROUP collaboration, *Review of particle physics*, *PTEP* **2022** (2022) 083C01 [INSPIRE].

[66] CLEO collaboration, *Absolute measurement of hadronic branching fractions of the D_s^+ meson*, *Phys. Rev. Lett.* **100** (2008) 161804 [`arXiv:0801.0680`] [INSPIRE].

[67] LHCb collaboration, *Prompt charm production in pp collisions at $\sqrt{s} = 7$ TeV*, *Nucl. Phys. B* **871** (2013) 1 [`arXiv:1302.2864`] [INSPIRE].

[68] LHCb collaboration, *Measurements of prompt charm production cross-sections in pp collisions at $\sqrt{s} = 13$ TeV*, *JHEP* **03** (2016) 159 [*Erratum ibid.* **09** (2016) 013] [`arXiv:1510.01707`] [INSPIRE].

[69] T. Skwarnicki, *A study of the radiative CASCADE transitions between the Upsilon-Prime and Upsilon resonances*, Ph.D. thesis, Institute of Nuclear Physics, Krakow, Poland (1986) [INSPIRE].

[70] A.D. Bukin, *Fitting function for asymmetric peaks*, `arXiv:0711.4449` [INSPIRE].

[71] K.S. Cranmer, *Kernel estimation in high-energy physics*, *Comput. Phys. Commun.* **136** (2001) 198 [`hep-ex/0011057`] [INSPIRE].

[72] LHCb collaboration, *Measurement of the track reconstruction efficiency at LHCb*, 2015 *JINST* **10** P02007 [`arXiv:1408.1251`] [INSPIRE].

[73] B. Ducloué, T. Lappi and H. Mäntysaari, *Forward J/ψ production in proton-nucleus collisions at high energy*, *Phys. Rev. D* **91** (2015) 114005 [`arXiv:1503.02789`] [INSPIRE].

[74] B. Ducloué, T. Lappi and H. Mäntysaari, *Forward J/ψ and D meson nuclear suppression at the LHC*, *Nucl. Part. Phys. Proc.* **289-290** (2017) 309 [`arXiv:1612.04585`] [INSPIRE].

[75] H. Fujii and K. Watanabe, *Nuclear modification of forward D production in pPb collisions at the LHC*, `arXiv:1706.06728` [INSPIRE].

[76] H.-S. Shao, *HELAC-Onia 2.0: an upgraded matrix-element and event generator for heavy quarkonium physics*, *Comput. Phys. Commun.* **198** (2016) 238 [`arXiv:1507.03435`] [INSPIRE].

[77] H.-S. Shao, *HELAC-Onia: an automatic matrix element generator for heavy quarkonium physics*, Comput. Phys. Commun. **184** (2013) 2562 [`arXiv:1212.5293`] [INSPIRE].

[78] J.-P. Lansberg and H.-S. Shao, *Towards an automated tool to evaluate the impact of the nuclear modification of the gluon density on quarkonium, D and B meson production in proton-nucleus collisions*, Eur. Phys. J. C **77** (2017) 1 [`arXiv:1610.05382`] [INSPIRE].

[79] A. Kusina, J.-P. Lansberg, I. Schienbein and H.-S. Shao, *Gluon shadowing in heavy-flavor production at the LHC*, Phys. Rev. Lett. **121** (2018) 052004 [`arXiv:1712.07024`] [INSPIRE].

[80] A. Kusina, J.-P. Lansberg, I. Schienbein and H.-S. Shao, *Reweighted nuclear PDFs using heavy-flavor production data at the LHC*, Phys. Rev. D **104** (2021) 014010 [`arXiv:2012.11462`] [INSPIRE].

[81] LHCb collaboration, *Measurement of the nuclear modification factor and prompt charged particle production in p-Pb and pp collisions at* $\sqrt{s_{\rm NN}} = 5$ *TeV*, Phys. Rev. Lett. **128** (2022) 142004 [`arXiv:2108.13115`] [INSPIRE].

[82] ALICE collaboration, *Charm-quark fragmentation fractions and production cross section at midrapidity in pp collisions at the LHC*, Phys. Rev. D **105** (2022) L011103 [`arXiv:2105.06335`] [INSPIRE].

The LHCb collaboration

R. Aaij[32], A.S.W. Abdelmotteleb[51], C. Abellan Beteta[45], F. Abudinén[51], T. Ackernley[55], B. Adeva[41], M. Adinolfi[49], P. Adlarson[77], H. Afsharnia[9], C. Agapopoulou[43], C.A. Aidala[78], Z. Ajaltouni[9], S. Akar[60], K. Akiba[32], P. Albicocco[23], J. Albrecht[15], F. Alessio[43], M. Alexander[54], A. Alfonso Albero[40], Z. Aliouche[57], P. Alvarez Cartelle[50], R. Amalric[13], S. Amato[2], J.L. Amey[49], Y. Amhis[11,43], L. An[5], L. Anderlini[22], M. Andersson[45], A. Andreianov[38], M. Andreotti[21], D. Andreou[63], D. Ao[6], F. Archilli[31,t], A. Artamonov[38], M. Artuso[63], E. Aslanides[10], M. Atzeni[45], B. Audurier[12], I. Bachiller Perea[8], S. Bachmann[17], M. Bachmayer[44], J.J. Back[51], A. Bailly-reyre[13], P. Baladron Rodriguez[41], V. Balagura[12], W. Baldini[21,43], J. Baptista de Souza Leite[1], M. Barbetti[22,k], I. R. Barbosa[65], R.J. Barlow[57], S. Barsuk[11], W. Barter[53], M. Bartolini[50], F. Baryshnikov[38], J.M. Basels[14], G. Bassi[29,q], B. Batsukh[4], A. Battig[15], A. Bay[44], A. Beck[51], M. Becker[15], F. Bedeschi[29], I.B. Bediaga[1], A. Beiter[63], S. Belin[41], V. Bellee[45], K. Belous[38], I. Belov[38], I. Belyaev[38], G. Benane[10], G. Bencivenni[23], E. Ben-Haim[13], A. Berezhnoy[38], R. Bernet[45], S. Bernet Andres[39], D. Berninghoff[17], H.C. Bernstein[63], C. Bertella[57], A. Bertolin[28], C. Betancourt[45], F. Betti[43], Ia. Bezshyiko[45], J. Bhom[35], L. Bian[69], M.S. Bieker[15], N.V. Biesuz[21], P. Billoir[13], A. Biolchini[32], M. Birch[56], F.C.R. Bishop[50], A. Bitadze[57], A. Bizzeti, M.P. Blago[50], T. Blake[51], F. Blanc[44], J.E. Blank[15], S. Blusk[63], D. Bobulska[54], V. Bocharnikov[38], J.A. Boelhauve[15], O. Boente Garcia[12], T. Boettcher[60], A. Boldyrev[38], C.S. Bolognani[75], R. Bolzonella[21,j], N. Bondar[38], F. Borgato[28], S. Borghi[57], M. Borsato[17], J.T. Borsuk[35], S.A. Bouchiba[44], T.J.V. Bowcock[55], A. Boyer[43], C. Bozzi[21], M.J. Bradley[56], S. Braun[61], A. Brea Rodriguez[41], N. Breer[15], J. Brodzicka[35], A. Brossa Gonzalo[41], J. Brown[55], D. Brundu[27], A. Buonaura[45], L. Buonincontri[28], A.T. Burke[57], C. Burr[43], A. Bursche[67], A. Butkevich[38], J.S. Butter[32], J. Buytaert[43], W. Byczynski[43], S. Cadeddu[27], H. Cai[69], R. Calabrese[21,j], L. Calefice[15], S. Cali[23], M. Calvi[26,n], M. Calvo Gomez[39], P. Campana[23], D.H. Campora Perez[75], A.F. Campoverde Quezada[6], S. Capelli[26,n], L. Capriotti[21], A. Carbone[20,h], R. Cardinale[24,l], A. Cardini[27], P. Carniti[26,n], L. Carus[17], A. Casais Vidal[41], R. Caspary[17], G. Casse[55], M. Cattaneo[43], G. Cavallero[21], V. Cavallini[21,j], S. Celani[44], J. Cerasoli[10], D. Cervenkov[58], A.J. Chadwick[55], I. Chahrour[78], M.G. Chapman[49], M. Charles[13], Ph. Charpentier[43], C.A. Chavez Barajas[55], M. Chefdeville[8], C. Chen[10], S. Chen[4], A. Chernov[35], S. Chernyshenko[47], V. Chobanova[41,w], S. Cholak[44], M. Chrzaszcz[35], A. Chubykin[38], V. Chulikov[38], P. Ciambrone[23], M.F. Cicala[51], X. Cid Vidal[41], G. Ciezarek[43], P. Cifra[43], P.E.L. Clarke[53], M. Clemencic[43], H.V. Cliff[50], J. Closier[43], J.L. Cobbledick[57], V. Coco[43], J. Cogan[10], E. Cogneras[9], L. Cojocariu[37], P. Collins[43], T. Colombo[43], A. Comerma-Montells[40], L. Congedo[19], A. Contu[27], N. Cooke[54], I. Corredoira [41], G. Corti[43], B. Couturier[43], D.C. Craik[45], M. Cruz Torres[1,f], R. Currie[53], C.L. Da Silva[62], S. Dadabaev[38], L. Dai[66], X. Dai[5], E. Dall'Occo[15], J. Dalseno[41], C. D'Ambrosio[43], J. Daniel[9], A. Danilina[38], P. d'Argent[19], J.E. Davies[57], A. Davis[57], O. De Aguiar Francisco[57], J. de Boer[43], K. De Bruyn[74], S. De Capua[57], M. De Cian[17], U. De Freitas Carneiro Da Graca[1], E. De Lucia[23], J.M. De Miranda[1], L. De Paula[2], M. De Serio[19,g], D. De Simone[45], P. De Simone[23], F. De Vellis[15], J.A. de Vries[75],

C.T. Dean[62], F. Debernardis[19,g], D. Decamp[8], V. Dedu[10], L. Del Buono[13], B. Delaney[59], H.-P. Dembinski[15], V. Denysenko[45], O. Deschamps[9], F. Dettori[27,i], B. Dey[72], P. Di Nezza[23], I. Diachkov[38], S. Didenko[38], S. Ding[63], V. Dobishuk[47], A. Dolmatov[38], C. Dong[3], A.M. Donohoe[18], F. Dordei[27], A.C. dos Reis[1], L. Douglas[54], A.G. Downes[8], P. Duda[76], M.W. Dudek[35], L. Dufour[43], V. Duk[73], P. Durante[43], M. M. Duras[76], J.M. Durham[62], D. Dutta[57], A. Dziurda[35], A. Dzyuba[38], S. Easo[52], U. Egede[64], A. Egorychev[38], V. Egorychev[38], C. Eirea Orro[41], S. Eisenhardt[53], E. Ejopu[57], S. Ek-In[44], L. Eklund[77], M. Elashri[60], J. Ellbracht[15], S. Ely[56], A. Ene[37], E. Epple[60], S. Escher[14], J. Eschle[45], S. Esen[45], T. Evans[57], F. Fabiano[27,i,43], L.N. Falcao[1], Y. Fan[6], B. Fang[11,69], L. Fantini[73,p], M. Faria[44], S. Farry[55], D. Fazzini[26,n], L. Felkowski[76], M. Feng[4,6], M. Feo[43], M. Fernandez Gomez[41], A.D. Fernez[61], F. Ferrari[20], L. Ferreira Lopes[44], F. Ferreira Rodrigues[2], S. Ferreres Sole[32], M. Ferrillo[45], M. Ferro-Luzzi[43], S. Filippov[38], R.A. Fini[19], M. Fiorini[21,j], M. Firlej[34], K.M. Fischer[58], D.S. Fitzgerald[78], C. Fitzpatrick[57], T. Fiutowski[34], F. Fleuret[12], M. Fontana[20], F. Fontanelli[24,l], R. Forty[43], D. Foulds-Holt[50], V. Franco Lima[55], M. Franco Sevilla[61], M. Frank[43], E. Franzoso[21,j], G. Frau[17], C. Frei[43], D.A. Friday[57], L. Frontini[25,m], J. Fu[6], Q. Fuehring[15], T. Fulghesu[13], E. Gabriel[32], G. Galati[19,g], M.D. Galati[32], A. Gallas Torreira[41], D. Galli[20,h], S. Gambetta[53,43], M. Gandelman[2], P. Gandini[25], H. Gao[6], R. Gao[58], Y. Gao[7], Y. Gao[5], M. Garau[27,i], L.M. Garcia Martin[44], P. Garcia Moreno[40], J. García Pardiñas[43], B. Garcia Plana[41], F.A. Garcia Rosales[12], L. Garrido[40], C. Gaspar[43], R.E. Geertsema[32], L.L. Gerken[15], E. Gersabeck[57], M. Gersabeck[57], T. Gershon[51], L. Giambastiani[28], V. Gibson[50], H.K. Giemza[36], A.L. Gilman[58], M. Giovannetti[23], A. Gioventù[41], P. Gironella Gironell[40], C. Giugliano[21,j], M.A. Giza[35], K. Gizdov[53], E.L. Gkougkousis[43], V.V. Gligorov[13], C. Göbel[65], E. Golobardes[39], D. Golubkov[38], A. Golutvin[56,38], A. Gomes[1,2,b,a,†], S. Gomez Fernandez[40], F. Goncalves Abrantes[58], M. Goncerz[35], G. Gong[3], I.V. Gorelov[38], C. Gotti[26], J.P. Grabowski[71], L.A. Granado Cardoso[43], E. Graugés[40], E. Graverini[44], G. Graziani, A. T. Grecu[37], L.M. Greeven[32], N.A. Grieser[60], L. Grillo[54], S. Gromov[38], C. Gu[12], M. Guarise[21,j], M. Guittiere[11], V. Guliaeva[38], P. A. Günther[17], A.K. Guseinov[38], E. Gushchin[38], Y. Guz[5,38,43], T. Gys[43], T. Hadavizadeh[64], C. Hadjivasiliou[61], G. Haefeli[44], C. Haen[43], J. Haimberger[43], S.C. Haines[50], T. Halewood-leagas[55], M.M. Halvorsen[43], P.M. Hamilton[61], J. Hammerich[55], Q. Han[7], X. Han[17], S. Hansmann-Menzemer[17], L. Hao[6], N. Harnew[58], T. Harrison[55], C. Hasse[43], M. Hatch[43], J. He[6,d], K. Heijhoff[32], F. Hemmer[43], C. Henderson[60], R.D.L. Henderson[64,51], A.M. Hennequin[59], K. Hennessy[55], L. Henry[43], J. Herd[56], J. Heuel[14], A. Hicheur[2], D. Hill[44], M. Hilton[57], S.E. Hollitt[15], J. Horswill[57], R. Hou[7], Y. Hou[8], J. Hu[17], J. Hu[67], W. Hu[5], X. Hu[3], W. Huang[6], X. Huang[69], W. Hulsbergen[32], R.J. Hunter[51], M. Hushchyn[38], D. Hutchcroft[55], P. Ibis[15], M. Idzik[34], D. Ilin[38], P. Ilten[60], A. Inglessi[38], A. Iniukhin[38], A. Ishteev[38], K. Ivshin[38], R. Jacobsson[43], H. Jage[14], S.J. Jaimes Elles[42,70], S. Jakobsen[43], E. Jans[32], B.K. Jashal[42], A. Jawahery[61], V. Jevtic[15], E. Jiang[61], X. Jiang[4,6], Y. Jiang[6], M. John[58], D. Johnson[59], C.R. Jones[50], T.P. Jones[51], S. Joshi[36], B. Jost[43], N. Jurik[43], I. Juszczak[35], S. Kandybei[46], Y. Kang[3], M. Karacson[43], D. Karpenkov[38], M. Karpov[38],

J.W. Kautz[60], F. Keizer[43], D.M. Keller[63], M. Kenzie[51], T. Ketel[32], B. Khanji[63], A. Kharisova[38], S. Kholodenko[38], G. Khreich[11], T. Kirn[14], V.S. Kirsebom[44], O. Kitouni[59], S. Klaver[33], N. Kleijne[29,q], K. Klimaszewski[36], M.R. Kmiec[36], S. Koliiev[47], L. Kolk[15], A. Kondybayeva[38], A. Konoplyannikov[38], P. Kopciewicz[34], R. Kopecna[17], P. Koppenburg[32], M. Korolev[38], I. Kostiuk[32], O. Kot[47], S. Kotriakhova, A. Kozachuk[38], P. Kravchenko[38], L. Kravchuk[38], M. Kreps[51], S. Kretzschmar[14], P. Krokovny[38], W. Krupa[34], W. Krzemien[36], J. Kubat[17], S. Kubis[76], W. Kucewicz[35], M. Kucharczyk[35], V. Kudryavtsev[38], E. Kulikova[38], A. Kupsc[77], D. Lacarrere[43], G. Lafferty[57], A. Lai[27], A. Lampis[27,i], D. Lancierini[45], C. Landesa Gomez[41], J.J. Lane[57], R. Lane[49], C. Langenbruch[17], J. Langer[15], O. Lantwin[38], T. Latham[51], F. Lazzari[29,r], C. Lazzeroni[48], R. Le Gac[10], S.H. Lee[78], R. Lefèvre[9], A. Leflat[38], S. Legotin[38], O. Leroy[10], T. Lesiak[35], B. Leverington[17], A. Li[3], H. Li[67], K. Li[7], P. Li[43], P.-R. Li[68], S. Li[7], T. Li[4], T. Li[67], Y. Li[4], Z. Li[63], Z. Lian[3], X. Liang[63], C. Lin[6], T. Lin[52], R. Lindner[43], V. Lisovskyi[44], R. Litvinov[27,i], G. Liu[67], H. Liu[6], K. Liu[68], Q. Liu[6], S. Liu[4,6], A. Lobo Salvia[40], A. Loi[27], R. Lollini[73], J. Lomba Castro[41], I. Longstaff[54], J.H. Lopes[2], A. Lopez Huertas[40], S. López Soliño[41], G.H. Lovell[50], Y. Lu[4,c], C. Lucarelli[22,k], D. Lucchesi[28,o], S. Luchuk[38], M. Lucio Martinez[75], V. Lukashenko[32,47], Y. Luo[3], A. Lupato[28], E. Luppi[21,j], K. Lynch[18], X.-R. Lyu[6], R. Ma[6], S. Maccolini[15], F. Machefert[11], F. Maciuc[37], I. Mackay[58], V. Macko[44], L.R. Madhan Mohan[50], A. Maevskiy[38], D. Maisuzenko[38], M.W. Majewski[34], J.J. Malczewski[35], S. Malde[58], B. Malecki[35,43], A. Malinin[38], T. Maltsev[38], G. Manca[27,i], G. Mancinelli[10], C. Mancuso[11,25,m], R. Manera Escalero[40], D. Manuzzi[20], C.A. Manzari[45], D. Marangotto[25,m], J.F. Marchand[8], U. Marconi[20], S. Mariani[43], C. Marin Benito[40], J. Marks[17], A.M. Marshall[49], P.J. Marshall[55], G. Martelli[73,p], G. Martellotti[30], L. Martinazzoli[43,n], M. Martinelli[26,n], D. Martinez Santos[41], F. Martinez Vidal[42], A. Massafferri[1], M. Materok[14], R. Matev[43], A. Mathad[45], V. Matiunin[38], C. Matteuzzi[63,26], K.R. Mattioli[12], A. Mauri[56], E. Maurice[12], J. Mauricio[40], M. Mazurek[43], M. McCann[56], L. Mcconnell[18], T.H. McGrath[57], N.T. McHugh[54], A. McNab[57], R. McNulty[18], B. Meadows[60], G. Meier[15], D. Melnychuk[36], S. Meloni[26,n], M. Merk[32,75], A. Merli[25,m], L. Meyer Garcia[2], D. Miao[4,6], H. Miao[6], M. Mikhasenko[71,e], D.A. Milanes[70], M. Milovanovic[43], M.-N. Minard[8,†], A. Minotti[26,n], E. Minucci[63], T. Miralles[9], S.E. Mitchell[53], B. Mitreska[15], D.S. Mitzel[15], A. Modak[52], A. Mödden[15], R.A. Mohammed[58], R.D. Moise[14], S. Mokhnenko[38], T. Mombächer[41], M. Monk[51,64], I.A. Monroy[70], S. Monteil[9], G. Morello[23], M.J. Morello[29,q], M.P. Morgenthaler[17], J. Moron[34], A.B. Morris[43], A.G. Morris[10], R. Mountain[63], H. Mu[3], E. Muhammad[51], F. Muheim[53], M. Mulder[74], K. Müller[45], D. Murray[57], R. Murta[56], P. Muzzetto[27,i], P. Naik[55], T. Nakada[44], R. Nandakumar[52], T. Nanut[43], I. Nasteva[2], M. Needham[53], N. Neri[25,m], S. Neubert[71], N. Neufeld[43], P. Neustroev[38], R. Newcombe[56], J. Nicolini[15,11], D. Nicotra[75], E.M. Niel[44], S. Nieswand[14], N. Nikitin[38], N.S. Nolte[59], C. Normand[8,i,27], J. Novoa Fernandez[41], G. Nowak[60], C. Nunez[78], A. Oblakowska-Mucha[34], V. Obraztsov[38], T. Oeser[14], S. Okamura[21,j], R. Oldeman[27,i], F. Oliva[53], M. Olocco[15], C.J.G. Onderwater[74], R.H. O'Neil[53], J.M. Otalora Goicochea[2], T. Ovsiannikova[38], P. Owen[45], A. Oyanguren[42], O. Ozcelik[53], K.O. Padeken[71], B. Pagare[51], P.R. Pais[43],

T. Pajero[58], A. Palano[19], M. Palutan[23], G. Panshin[38], L. Paolucci[51], A. Papanestis[52], M. Pappagallo[19,g], L.L. Pappalardo[21,j], C. Pappenheimer[60], C. Parkes[57,43], B. Passalacqua[21,j], G. Passaleva[22], A. Pastore[19], M. Patel[56], C. Patrignani[20,h], C.J. Pawley[75], A. Pellegrino[32], M. Pepe Altarelli[23], S. Perazzini[20], D. Pereima[38], A. Pereiro Castro[41], P. Perret[9], K. Petridis[49], A. Petrolini[24,l], S. Petrucci[53], M. Petruzzo[25], H. Pham[63], A. Philippov[38], R. Piandani[6], L. Pica[29,q], M. Piccini[73], B. Pietrzyk[8], G. Pietrzyk[11], D. Pinci[30], F. Pisani[43], M. Pizzichemi[26,n,43], V. Placinta[37], J. Plews[48], M. Plo Casasus[41], F. Polci[13,43], M. Poli Lener[23], A. Poluektov[10], N. Polukhina[38], I. Polyakov[43], E. Polycarpo[2], S. Ponce[43], D. Popov[6,43], S. Poslavskii[38], K. Prasanth[35], L. Promberger[17], C. Prouve[41], V. Pugatch[47], V. Puill[11], G. Punzi[29,r], H.R. Qi[3], W. Qian[6], N. Qin[3], S. Qu[3], R. Quagliani[44], B. Rachwal[34], J.H. Rademacker[49], R. Rajagopalan[63], M. Rama[29], M. Ramos Pernas[51], M.S. Rangel[2], F. Ratnikov[38], G. Raven[33], M. Rebollo De Miguel[42], F. Redi[43], J. Reich[49], F. Reiss[57], Z. Ren[3], P.K. Resmi[58], R. Ribatti[29,q], A.M. Ricci[27], S. Ricciardi[52], K. Richardson[59], M. Richardson-Slipper[53], K. Rinnert[55], P. Robbe[11], G. Robertson[53], E. Rodrigues[55,43], E. Rodriguez Fernandez[41], J.A. Rodriguez Lopez[70], E. Rodriguez Rodriguez[41], D.L. Rolf[43], A. Rollings[58], P. Roloff[43], V. Romanovskiy[38], M. Romero Lamas[41], A. Romero Vidal[41], M. Rotondo[23], M.S. Rudolph[63], T. Ruf[43], R.A. Ruiz Fernandez[41], J. Ruiz Vidal[42], A. Ryzhikov[38], J. Ryzka[34], J.J. Saborido Silva[41], N. Sagidova[38], N. Sahoo[48], B. Saitta[27,i], M. Salomoni[43], C. Sanchez Gras[32], I. Sanderswood[42], R. Santacesaria[30], C. Santamarina Rios[41], M. Santimaria[23], L. Santoro[1], E. Santovetti[31], D. Saranin[38], G. Sarpis[53], M. Sarpis[71], A. Sarti[30], C. Satriano[30,s], A. Satta[31], M. Saur[5], D. Savrina[38], H. Sazak[9], L.G. Scantlebury Smead[58], A. Scarabotto[13], S. Schael[14], S. Scherl[55], A. M. Schertz[72], M. Schiller[54], H. Schindler[43], M. Schmelling[16], B. Schmidt[43], S. Schmitt[14], O. Schneider[44], A. Schopper[43], M. Schubiger[32], N. Schulte[15], S. Schulte[44], M.H. Schune[11], R. Schwemmer[43], G. Schwering[14], B. Sciascia[23], A. Sciuccati[43], S. Sellam[41], A. Semennikov[38], M. Senghi Soares[33], A. Sergi[24,l], N. Serra[45,43], L. Sestini[28], A. Seuthe[15], Y. Shang[5], D.M. Shangase[78], M. Shapkin[38], I. Shchemerov[38], L. Shchutska[44], T. Shears[55], L. Shekhtman[38], Z. Shen[5], S. Sheng[4,6], V. Shevchenko[38], B. Shi[6], E.B. Shields[26,n], Y. Shimizu[11], E. Shmanin[38], R. Shorkin[38], J.D. Shupperd[63], B.G. Siddi[21,j], R. Silva Coutinho[63], G. Simi[28], S. Simone[19,g], M. Singla[64], N. Skidmore[57], R. Skuza[17], T. Skwarnicki[63], M.W. Slater[48], J.C. Smallwood[58], J.G. Smeaton[50], E. Smith[59], K. Smith[62], M. Smith[56], A. Snoch[32], L. Soares Lavra[53], M.D. Sokoloff[60], F.J.P. Soler[54], A. Solomin[38,49], A. Solovev[38], I. Solovyev[38], R. Song[64], Y. Song[3], F.L. Souza De Almeida[2], B. Souza De Paula[2], E. Spadaro Norella[25,m], E. Spedicato[20], J.G. Speer[15], E. Spiridenkov[38], P. Spradlin[54], V. Sriskaran[43], F. Stagni[43], M. Stahl[43], S. Stahl[43], S. Stanislaus[58], E.N. Stein[43], O. Steinkamp[45], O. Stenyakin[38], H. Stevens[15], D. Strekalina[38], Y. Su[6], F. Suljik[58], J. Sun[27], L. Sun[69], Y. Sun[61], P.N. Swallow[48], K. Swientek[34], A. Szabelski[36], T. Szumlak[34], M. Szymanski[43], Y. Tan[3], S. Taneja[57], M.D. Tat[58], A. Terentev[45], F. Teubert[43], E. Thomas[43], D.J.D. Thompson[48], H. Tilquin[56], V. Tisserand[9], S. T'Jampens[8], M. Tobin[4], L. Tomassetti[21,j], G. Tonani[25,m], X. Tong[5], D. Torres Machado[1], L. Toscano[15], D.Y. Tou[3], C. Trippl[44], G. Tuci[17], N. Tuning[32],

A. Ukleja[36], D.J. Unverzagt[17], E. Ursov[38], A. Usachov[33], A. Ustyuzhanin[38], U. Uwer[17], V. Vagnoni[20], A. Valassi[43], G. Valenti[20], N. Valls Canudas[39], M. Van Dijk[44], H. Van Hecke[62], E. van Herwijnen[56], C.B. Van Hulse[41,v], M. van Veghel[32], R. Vazquez Gomez[40], P. Vazquez Regueiro[41], C. Vázquez Sierra[41], S. Vecchi[21], J.J. Velthuis[49], M. Veltri[22,u], A. Venkateswaran[44], M. Vesterinen[51], D. Vieira[60], M. Vieites Diaz[44], X. Vilasis-Cardona[39], E. Vilella Figueras[55], A. Villa[20], P. Vincent[13], F.C. Volle[11], D. vom Bruch[10], V. Vorobyev[38], N. Voropaev[38], K. Vos[75], C. Vrahas[53], J. Walsh[29], E.J. Walton[64], G. Wan[5], C. Wang[17], G. Wang[7], J. Wang[5], J. Wang[4], J. Wang[3], J. Wang[69], M. Wang[25], R. Wang[49], X. Wang[67], Y. Wang[7], Z. Wang[45], Z. Wang[3], Z. Wang[6], J.A. Ward[51,64], N.K. Watson[48], D. Websdale[56], Y. Wei[5], B.D.C. Westhenry[49], D.J. White[57], M. Whitehead[54], A.R. Wiederhold[51], D. Wiedner[15], G. Wilkinson[58], M.K. Wilkinson[60], I. Williams[50], M. Williams[59], M.R.J. Williams[53], R. Williams[50], F.F. Wilson[52], W. Wislicki[36], M. Witek[35], L. Witola[17], C.P. Wong[62], G. Wormser[11], S.A. Wotton[50], H. Wu[63], J. Wu[7], Y. Wu[5], K. Wyllie[43], Z. Xiang[6], Y. Xie[7], A. Xu[29], J. Xu[6], L. Xu[3], L. Xu[3], M. Xu[51], Q. Xu[6], Z. Xu[9], Z. Xu[6], Z. Xu[4], D. Yang[3], S. Yang[6], X. Yang[5], Y. Yang[24], Z. Yang[5], Z. Yang[61], V. Yeroshenko[11], H. Yeung[57], H. Yin[7], J. Yu[66], X. Yuan[4], E. Zaffaroni[44], M. Zavertyaev[16], M. Zdybal[35], M. Zeng[3], C. Zhang[5], D. Zhang[7], J. Zhang[6], L. Zhang[3], S. Zhang[66], S. Zhang[5], Y. Zhang[5], Y. Zhang[58], Y. Zhao[17], A. Zharkova[38], A. Zhelezov[17], Y. Zheng[6], T. Zhou[5], X. Zhou[7], Y. Zhou[6], V. Zhovkovska[11], L. Z. Zhu[6], X. Zhu[3], X. Zhu[7], Z. Zhu[6], V. Zhukov[14,38], J. Zhuo[42], Q. Zou[4,6], S. Zucchelli[20,h], D. Zuliani[28], G. Zunica[57]

[1] *Centro Brasileiro de Pesquisas Físicas (CBPF), Rio de Janeiro, Brazil*
[2] *Universidade Federal do Rio de Janeiro (UFRJ), Rio de Janeiro, Brazil*
[3] *Center for High Energy Physics, Tsinghua University, Beijing, China*
[4] *Institute Of High Energy Physics (IHEP), Beijing, China*
[5] *School of Physics State Key Laboratory of Nuclear Physics and Technology, Peking University, Beijing, China*
[6] *University of Chinese Academy of Sciences, Beijing, China*
[7] *Institute of Particle Physics, Central China Normal University, Wuhan, Hubei, China*
[8] *Université Savoie Mont Blanc, CNRS, IN2P3-LAPP, Annecy, France*
[9] *Université Clermont Auvergne, CNRS/IN2P3, LPC, Clermont-Ferrand, France*
[10] *Aix Marseille Univ, CNRS/IN2P3, CPPM, Marseille, France*
[11] *Université Paris-Saclay, CNRS/IN2P3, IJCLab, Orsay, France*
[12] *Laboratoire Leprince-Ringuet, CNRS/IN2P3, Ecole Polytechnique, Institut Polytechnique de Paris, Palaiseau, France*
[13] *LPNHE, Sorbonne Université, Paris Diderot Sorbonne Paris Cité, CNRS/IN2P3, Paris, France*
[14] *I. Physikalisches Institut, RWTH Aachen University, Aachen, Germany*
[15] *Fakultät Physik, Technische Universität Dortmund, Dortmund, Germany*
[16] *Max-Planck-Institut für Kernphysik (MPIK), Heidelberg, Germany*
[17] *Physikalisches Institut, Ruprecht-Karls-Universität Heidelberg, Heidelberg, Germany*
[18] *School of Physics, University College Dublin, Dublin, Ireland*
[19] *INFN Sezione di Bari, Bari, Italy*
[20] *INFN Sezione di Bologna, Bologna, Italy*
[21] *INFN Sezione di Ferrara, Ferrara, Italy*
[22] *INFN Sezione di Firenze, Firenze, Italy*
[23] *INFN Laboratori Nazionali di Frascati, Frascati, Italy*
[24] *INFN Sezione di Genova, Genova, Italy*

[25] *INFN Sezione di Milano, Milano, Italy*
[26] *INFN Sezione di Milano-Bicocca, Milano, Italy*
[27] *INFN Sezione di Cagliari, Monserrato, Italy*
[28] *Università degli Studi di Padova, Università e INFN, Padova, Padova, Italy*
[29] *INFN Sezione di Pisa, Pisa, Italy*
[30] *INFN Sezione di Roma La Sapienza, Roma, Italy*
[31] *INFN Sezione di Roma Tor Vergata, Roma, Italy*
[32] *Nikhef National Institute for Subatomic Physics, Amsterdam, Netherlands*
[33] *Nikhef National Institute for Subatomic Physics and VU University Amsterdam, Amsterdam, Netherlands*
[34] *AGH — University of Science and Technology, Faculty of Physics and Applied Computer Science, Kraków, Poland*
[35] *Henryk Niewodniczanski Institute of Nuclear Physics Polish Academy of Sciences, Kraków, Poland*
[36] *National Center for Nuclear Research (NCBJ), Warsaw, Poland*
[37] *Horia Hulubei National Institute of Physics and Nuclear Engineering, Bucharest-Magurele, Romania*
[38] *Affiliated with an institute covered by a cooperation agreement with CERN*
[39] *DS4DS, La Salle, Universitat Ramon Llull, Barcelona, Spain*
[40] *ICCUB, Universitat de Barcelona, Barcelona, Spain*
[41] *Instituto Galego de Física de Altas Enerxías (IGFAE), Universidade de Santiago de Compostela, Santiago de Compostela, Spain*
[42] *Instituto de Fisica Corpuscular, Centro Mixto Universidad de Valencia — CSIC, Valencia, Spain*
[43] *European Organization for Nuclear Research (CERN), Geneva, Switzerland*
[44] *Institute of Physics, Ecole Polytechnique Fédérale de Lausanne (EPFL), Lausanne, Switzerland*
[45] *Physik-Institut, Universität Zürich, Zürich, Switzerland*
[46] *NSC Kharkiv Institute of Physics and Technology (NSC KIPT), Kharkiv, Ukraine*
[47] *Institute for Nuclear Research of the National Academy of Sciences (KINR), Kyiv, Ukraine*
[48] *University of Birmingham, Birmingham, United Kingdom*
[49] *H.H. Wills Physics Laboratory, University of Bristol, Bristol, United Kingdom*
[50] *Cavendish Laboratory, University of Cambridge, Cambridge, United Kingdom*
[51] *Department of Physics, University of Warwick, Coventry, United Kingdom*
[52] *STFC Rutherford Appleton Laboratory, Didcot, United Kingdom*
[53] *School of Physics and Astronomy, University of Edinburgh, Edinburgh, United Kingdom*
[54] *School of Physics and Astronomy, University of Glasgow, Glasgow, United Kingdom*
[55] *Oliver Lodge Laboratory, University of Liverpool, Liverpool, United Kingdom*
[56] *Imperial College London, London, United Kingdom*
[57] *Department of Physics and Astronomy, University of Manchester, Manchester, United Kingdom*
[58] *Department of Physics, University of Oxford, Oxford, United Kingdom*
[59] *Massachusetts Institute of Technology, Cambridge, MA, United States*
[60] *University of Cincinnati, Cincinnati, OH, United States*
[61] *University of Maryland, College Park, MD, United States*
[62] *Los Alamos National Laboratory (LANL), Los Alamos, NM, United States*
[63] *Syracuse University, Syracuse, NY, United States*
[64] *School of Physics and Astronomy, Monash University, Melbourne, Australia, associated to* [51]
[65] *Pontifícia Universidade Católica do Rio de Janeiro (PUC-Rio), Rio de Janeiro, Brazil, associated to* [2]
[66] *Physics and Micro Electronic College, Hunan University, Changsha City, China, associated to* [7]
[67] *Guangdong Provincial Key Laboratory of Nuclear Science, Guangdong-Hong Kong Joint Laboratory of Quantum Matter, Institute of Quantum Matter, South China Normal University, Guangzhou, China, associated to* [3]
[68] *Lanzhou University, Lanzhou, China, associated to* [4]
[69] *School of Physics and Technology, Wuhan University, Wuhan, China, associated to* [3]
[70] *Departamento de Fisica, Universidad Nacional de Colombia, Bogota, Colombia, associated to* [13]
[71] *Universität Bonn — Helmholtz-Institut für Strahlen und Kernphysik, Bonn, Germany, associated to* [17]
[72] *Eotvos Lorand University, Budapest, Hungary, associated to* [43]
[73] *INFN Sezione di Perugia, Perugia, Italy, associated to* [21]

[74] *Van Swinderen Institute, University of Groningen, Groningen, Netherlands, associated to* [32]
[75] *Universiteit Maastricht, Maastricht, Netherlands, associated to* [32]
[76] *Tadeusz Kosciuszko Cracow University of Technology, Cracow, Poland, associated to* [35]
[77] *Department of Physics and Astronomy, Uppsala University, Uppsala, Sweden, associated to* [54]
[78] *University of Michigan, Ann Arbor, MI, United States, associated to* [63]

[a] *Universidade de Brasília, Brasília, Brazil*
[b] *Universidade Federal do Triângulo Mineiro (UFTM), Uberaba-MG, Brazil*
[c] *Central South U., Changsha, China*
[d] *Hangzhou Institute for Advanced Study, UCAS, Hangzhou, China*
[e] *Excellence Cluster ORIGINS, Munich, Germany*
[f] *Universidad Nacional Autónoma de Honduras, Tegucigalpa, Honduras*
[g] *Università di Bari, Bari, Italy*
[h] *Università di Bologna, Bologna, Italy*
[i] *Università di Cagliari, Cagliari, Italy*
[j] *Università di Ferrara, Ferrara, Italy*
[k] *Università di Firenze, Firenze, Italy*
[l] *Università di Genova, Genova, Italy*
[m] *Università degli Studi di Milano, Milano, Italy*
[n] *Università di Milano Bicocca, Milano, Italy*
[o] *Università di Padova, Padova, Italy*
[p] *Università di Perugia, Perugia, Italy*
[q] *Scuola Normale Superiore, Pisa, Italy*
[r] *Università di Pisa, Pisa, Italy*
[s] *Università della Basilicata, Potenza, Italy*
[t] *Università di Roma Tor Vergata, Roma, Italy*
[u] *Università di Urbino, Urbino, Italy*
[v] *Universidad de Alcalá, Alcalá de Henares, Spain*
[w] *Universidade da Coruña, Coruña, Spain*
† *Deceased*